Microbiome

RESEARCH

Open Access

Faecalibacterium prausnitzii-derived outer membrane vesicles reprogram gut microbiota metabolism to alleviate Porcine Epidemic Diarrhea Virus infection

JunHong Xing[1†], TianMing Niu[1†], Tong Yu[1†], BoShi Zou[1], ChunWei Shi[1], YingJie Wang[1], ShuHui Fan[1], MingHan Li[1], MeiYing Bao[1], Yu Sun[1], KuiPeng Gao[1], JingJing Qiu[1], DongXing Zhang[1], Nan Wang[1], YanLong Jiang[1], HaiBin Huang[1], Xin Cao[1], Yan Zeng[1], JianZhong Wang[1], ShuMin Zhang[1], JingTao Hu[1], Di Zhang[1], WuSheng Sun[1], GuiLian Yang[1*], WenTao Yang[1*] and ChunFeng Wang[1*]

Abstract

Background The Porcine Epidemic Diarrhea Virus (PEDV) is one of the major challenges facing the global pig farming industry, and vaccines and treatments have proven difficult in controlling its spread. *Faecalibacterium prausnitzii* (*F. prausnitzii*), a key commensal bacterium in the gut, has been recognized as a promising candidate for next-generation probiotics due to its potential wide-ranging health benefits. A decrease in *F.prausnitzii* abundance has been associated with certain viral infections, suggesting its potential application in preventing intestinal viral infections. In this study, we utilized a piglet model to examine the potential role of *F.prausnitzii* in PEDV infections.

Results A piglet model of PEDV infection was established and supplemented with *F.prausnitzii*, revealing that *F. prausnitzii* mitigated PEDV infection. Further studies found that outer membrane vesicles (OMVs) are the main functional components of *F.prausnitzii*, and proteomics, untargeted metabolomics, and small RNA-seq were used to analyze the composition of OMVs. Exhaustion of the gut microbiota demonstrated that the function of Fp. OMVs relies on the presence of the gut microbiota. Additionally, metagenomic analysis indicated that Fp. OMVs altered the gut microbiota composition, enhancing the abundance of *Faecalibacterium prausnitzii*, *Prevotellamassilia timonensis*, and *Limosilactobacillus reuteri*. Untargeted metabolomics analysis showed that Fp. OMVs increased phosphatidylcholine (PC) levels, with PC identified as a key metabolite in alleviating PEDV infection. Single-cell sequencing revealed that PC altered the relative abundance of intestinal cells, increased the number of intestinal epithelial cells, and reduced necroptosis in target cells. PC treatment in infected IPEC-J2 and Vero cells alleviated necroptosis and reduced the activation of the RIPK1-RIPK3-MLKL signaling axis, thereby improving PEDV infection.

Conclusion *F.prausnitzii* and its OMVs play a critical role in mitigating PEDV infections. These findings provide a promising strategy to ameliorate PEDV infection in piglets.

[†]JunHong Xing, TianMing Niu and Tong Yu contributed equally to this work.

*Correspondence:
GuiLian Yang
yangguilian@jlau.edu.cn
WenTao Yang
yangwentao@jlau.edu.cn
ChunFeng Wang
wangchunfeng@jlau.edu.cn

Keywords PEDV, *F.prausnitzii*, OMVs, Gut microbiota, Phosphatidylcholine

Graphical Abstract

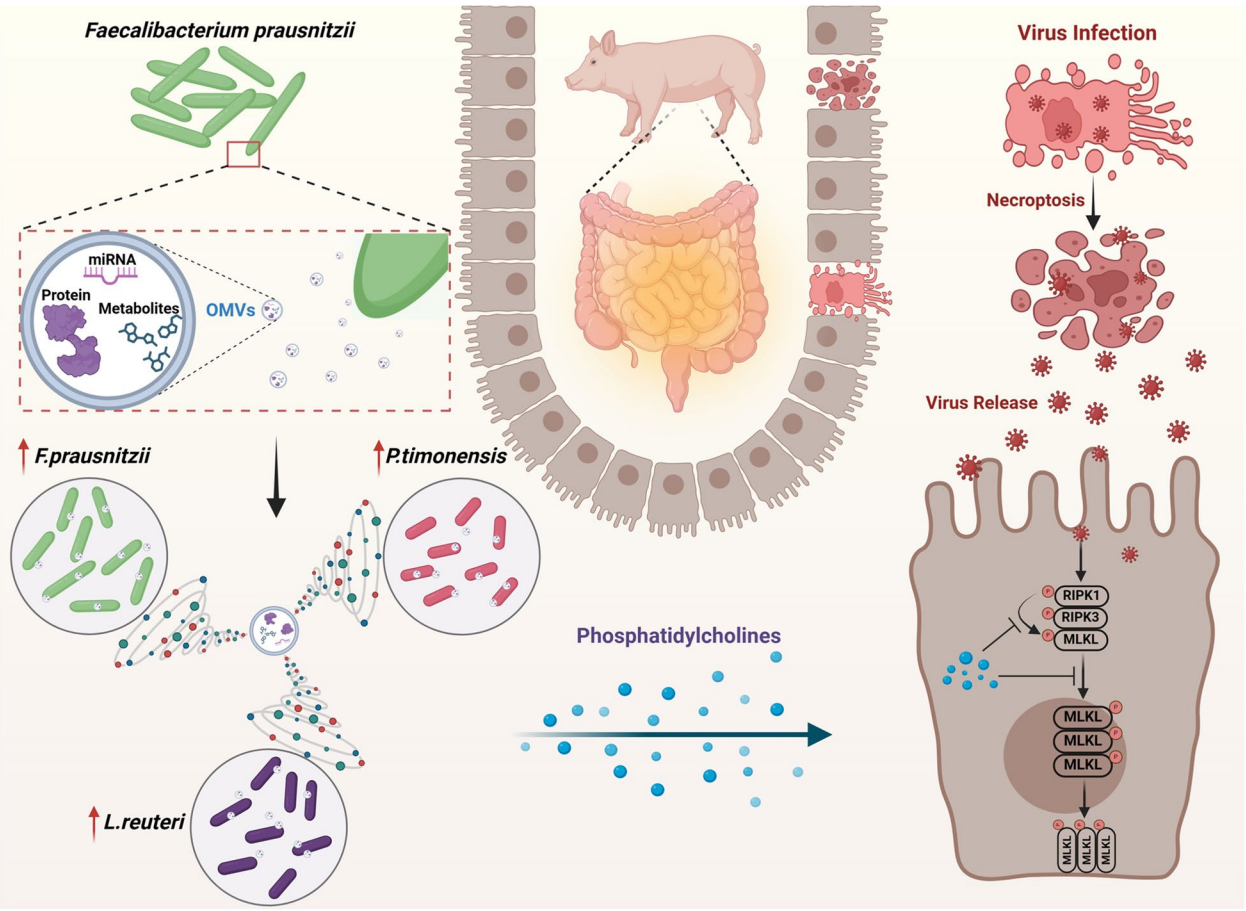

Introduction

Porcine Epidemic Diarrhea Virus (PEDV) is a virus that causes highly contagious diarrhea, posing a particularly lethal threat to piglets. Since its initial identification in the 1970s, PEDV outbreaks have continuously spread globally, significantly impacting productivity in the swine industry [1]. Due to PEDV's high pathogenicity and rapid transmission rate, outbreaks typically lead to widespread piglet mortality, resulting in substantial economic losses for pig farming operations. Furthermore, the limited efficacy of current vaccines and treatment options exacerbates the challenges of epidemic prevention and control [2]. *F.prausnitzii* has drawn widespread interest for its potential in regulating inflammatory responses and supporting gut health [3]. Numerous studies have shown a close association between *F.prausnitzii* abundance and gut health, particularly in patients with inflammatory bowel disease (IBD), where its levels are notably reduced [4]. Analysis of the gut microbiota in Crohn's Disease patients identified *F.prausnitzii* as an anti-inflammatory symbiont that, when supplemented, effectively alleviates the disease and improves inflammatory responses [5]. Additionally, *F.prausnitzii* mediates GPR43 signaling via butyrate production, aiding CKD renal recovery [6]. The abundance of *F.prausnitzii* is significantly reduced in certain viral infection states [7–13], and while previous studies have highlighted its role in inflammation regulation, the specific mechanisms underlying its function during viral infections remain underexplored, limiting its potential applications in antiviral therapy.

The gut microbiota is pivotal in regulating the host's immune responses, with certain probiotics found to

inhibit viral replication and reduce viral infection symptoms by boosting the host's innate immune response [14]. Bacterial OMVs are crucial in host–pathogen interactions. Secreted by Gram-negative bacteria, OMVs are small vesicles containing various bioactive substances, including proteins, lipids, DNA, and RNA [15]. OMVs from *Helicobacter pylori* may promote the passage of bacterial antigens through the gastric epithelial barrier, contributing to local and systemic host inflammation and immune responses [16]. Moreover, OMVs play a role in gene-level exchange between bacteria and between bacteria and hosts [17, 18]. For instance, OMVs from *Klebsiella pneumoniae* can transfer plasmids containing resistance genes to *Escherichia coli*, *Salmonella enterica*, and *Pseudomonas aeruginosa*, impacting microbiota antibiotic sensitivity and potentially altering host metabolism and immune responses [19]. In a mouse model, OMVs from *Akkermansia muciniphila* promote placental formation and alleviate preeclampsia [20]. Similarly, extracellular vesicles from *Lactobacillus johnsonii* and *Lactobacillus plantarum* promote M2 macrophage polarization to combat inflammation [21, 22].

Metabolites produced by the gut microbiota play crucial roles in host health and disease, with metabolomics studies highlighting their diverse functions in regulating host physiological processes [23]. Research indicates that short-chain fatty acids (SCFAs) produced by the gut microbiota regulate host immune and inflammatory responses by activating G protein-coupled receptors, such as GPR41 and GPR43 [24, 25]. Similarly, secondary bile acids influence host metabolic pathways and immune responses by activating the farnesoid X receptor (FXR) and the TGR5 receptor [26]. Another significant class of gut microbial metabolites includes indole and its derivatives. Indole-3-propionic acid promotes aryl hydrocarbon receptor (AhR) production, inhibits NF-κB signaling and NLRP3 inflammasome formation, and mitigates inflammation [27]. Phosphatidylcholine, a primary membrane-forming phospholipid in eukaryotes, is synthesized through the methylation pathway or the CDP-choline pathway and is also involved in interactions between macrophages and lymphocytes [28].

This study aims to reveal the role of *F.prausnitzii* in PEDV infections. We demonstrate that *F.prausnitzii* can improve viral infections through mechanisms mediated by its OMVs. These Fp.OMVs regulate the structural composition and metabolic profiles of the gut microbiota, with PC being a key metabolite that influences the distribution of intestinal cell subpopulations. Furthermore, Fp.OMVs reduce extensive necroptosis of target cells caused by viral infections, thereby minimizing tissue damage. This finding provides a strategy for PEDV prevention and treatment.

Methods

Cells, bacteria, and virus

Vero cells and IPEC-J2 cells were cultured in DMEM and DMEM/F12, respectively (Servicebio, China), with the addition of 10% fetal bovine serum (Gibco, USA) at 37 °C in a 5% CO_2 environment. *Faecalibacterium prausnitzii*, *Prevotellamassilia timonensis*, and *Limosilactobacillus reuteri* were maintained in our laboratory, with standard strain numbers DSM107840, DSM22865, and CICC6123, respectively. *Faecalibacterium prausnitzii* was cultured in BHI medium, *Prevotellamassilia timonensis* in DSM Medium 110, and *Limosilactobacillus reuteri* in MRS medium under anaerobic conditions at 37 °C. PEDV CV777 was kept in our laboratory and propagated using Vero cells. The viral units used in this study were $10^{4.344}$ PFU ml^{-1}.

Animals and experimental design

The Landrace pigs were sourced from a farm in Jilin Province, China. The piglets were weaned after consuming colostrum for three days and were subsequently fed with artificial formula milk to ensure uniform nutrient intake for all piglets. During group assignment, piglets from the same litter were evenly distributed across different experimental groups to minimize the effect of maternal milk variability on individual groups. The diet and environmental conditions were kept consistent for all piglets, with each experimental group housed separately. The environmental temperature was maintained at 28–30 °C, with humidity levels between 50–70%. All piglets tested negative for PEDV. The study comprised four segments: *F.prausnitzii* functionality experiments, effector substance functionality experiments, gut microbiota depletion experiments, and PC functionality experiments. Parallel experiments were conducted in each segment for sample collection.

In the first part, piglets were randomly assigned to three groups: Fp + PEDV ($n = 8$), PEDV ($n = 8$), and Control ($n = 5$). The Fp + PEDV group received *F.prausnitzii* (10^9 CFU/kg) once a day from days 0 to 7, and both the Fp + PEDV and PEDV groups were challenged with PEDV on day 7.

In the second part, piglets were randomly divided into five groups: Fp.supernatant + PEDV ($n = 6$), Fp.inactivated + PEDV ($n = 6$), Fp.OMVs + PEDV ($n = 6$), PEDV ($n = 6$), and Control ($n = 6$). The Fp.supernatant + PEDV, Fp.inactivated + PEDV, and Fp.OMVs + PEDV groups were administered *F.prausnitzii* culture supernatant (50kD filtration extraction), inactivated *F.prausnitzii* (10^9 CFU/kg), and Fp.OMVs (1 mg/kg) once a day from days 0 to 7, respectively. All groups except the Control were challenged with PEDV on day 7.

In the third part, piglets were randomly assigned to four groups: Abx + Fp.OMVs + PEDV ($n=6$), Fp.OMVs + PEDV ($n=6$), PEDV ($n=6$), and Control ($n=6$). The Abx + Fp.OMVs + PEDV group received antibiotic treatment from days 0 to 5, and both the Abx + Fp.OMVs + PEDV and Fp.OMVs + PEDV groups were administered Fp.OMVs (1 mg/kg) once a day from days 5 to 12. All groups except the Control were challenged with PEDV on day 12.

In the fourth part, piglets were randomly allocated into three groups: Abx + PC + PEDV ($n=6$), Abx + PEDV ($n=6$), and Control ($n=6$). The Abx + PC + PEDV and Abx + PEDV groups received antibiotic treatment from days 0 to 5, and the Abx + PC + PEDV group was given PC (10 mg/kg) (Medchemexpress, USA) once a day from days 5 to 12. All groups except the Control were challenged with PEDV on day 12. Throughout all experiments, piglets in the Control group were administered PBS at all stages. All experiments involved orally gavaging 1 ml of PEDV ($10^{4.344}$ PFU ml^{-1}) to piglets, followed by assessment of body weight changes, survival, diarrhea, and viral load over the next 7 days to characterize the infection state. Intestinal contents samples from piglets in the Fp.OMVs + PEDV group and the PEDV group were collected during the second and third parts of the animal experiments for subsequent metagenomic and untargeted metabolomic analyses.

Antibiotic treatment

Ampicillin (1 mg/ml) (Solarbio, China), streptomycin (1 mg/ml) (Solarbio, China), vancomycin (0.25 mg/ml) (Solarbio, China), and neomycin (1 mg/ml) (Solarbio, China) were incorporated into the milk and administered for 5 days to extensively reduce the gut microbial background of the piglets [29].

Bacterial outer membrane vesicle isolation

F.prausnitzii was cultured anaerobically, and the supernatant was collected during the logarithmic growth phase. The supernatant was filtered through a 0.22 μm filter, transferred to a 50 kD centrifugal filter unit, and centrifuged at 10,000 × g for 50 min. The filtrate was then transferred to a centrifuge tube for ultracentrifugation at 120,000 × g for 120 min. The OMVs were collected from the tube's bottom, resuspended in 1 ml PBS, and stored at −80 °C after concentration determination [30].

Bacterial inactivation treatment

After bacterial culture, the suspension was collected and washed three times with PBS. The suspension was then inactivated at 70 °C for 30 min, followed by three additional PBS washes for subsequent studies.

Fp.OMVs proteomics

Samples were treated with Denaturing Buffer, centrifuged at 12,000 × g for 15 min at 4 °C, and the supernatant was collected. It was then treated with 1 M DTT at 56 °C for 1 h, followed by incubation with Iodoacetamide at room temperature in the dark for 1 h. Formalin-Fixed, Paraffin-Embedded samples were dewaxed with octane, rehydrated with ethanol, washed in PBS, and incubated with protein lysis buffer (4% SDS, 100 mM Tris) at 95 °C for 10 min. After sonication and incubation at 95 °C for 60 min, Tris (2-carboxyethyl) phosphine and Chloroacetamide were added for reduction and alkylation. The supernatant was centrifuged, precipitated with acetone at −20 °C for at least 4 h, and dissolved in lysis buffer. Protein concentrations were measured by the Bradford assay, and 20 μg of protein was analyzed using SDS-PAGE (12%) stained with Coomassie Brilliant Blue. Proteins were digested with trypsin at 37 °C for 4 h, followed by overnight digestion with trypsin and $CaCl_2$. The pH was adjusted with formic acid, centrifuged, and desalted using a C18 column. The eluate was freeze-dried. Liquid chromatography was performed using a Vanquish Neo UHPLC system, followed by mass spectrometry in data-dependent acquisition mode. Functional protein analysis, including GO, IPR, COG, and KEGG pathways, was done using InterProScan software.

Fp.OMVs small RNA-seq

OMVs samples were mixed with RNA lysis buffer and incubated at room temperature for 5 min, followed by the addition of 140 μl chloroform. After vortexing and incubation, the mixture was centrifuged at 12,000 × g for 15 min at 4 °C. The aqueous phase was collected, mixed with ethanol, and passed through an RNeasy spin column. After washing with Buffer RWT and Buffer RPE, RNA was eluted with RNase-free water and stored at −80 °C. RNA quantification was performed using a Quantus Fluorometer. For 3' and 5' adaptor ligation, reactions were incubated at 28 °C, followed by cycling at 65 °C and 4 °C. cDNA synthesis and purification were done using QMN Beads, followed by PCR amplification. miRNA libraries were sequenced using PE150 sequencing. FastQC and Fastp were used for quality assessment and trimming. Bowtie was used to align sequences to the Rfam database to remove rRNA and ncRNA, and the miRBase database was used for miRNA identification.

Metagenome assembly and functional annotations

Total DNA was extracted using the Fecal Genome DNA Extraction Kit (BioTeke, China). Libraries were constructed using the TruSeq Nano DNA Library Preparation Kit (Illumina, USA) and sequenced on an Illumina

NovaSeq 6000 platform with 150 bp paired-end reads. Adapters and low-quality reads were removed using cutadapt and fqtrim, and the remaining reads were aligned with bowtie and assembled using MEGAHIT. Coding sequences were predicted with MetaGeneMark and clustered into unigenes using CD-HIT. LEfSe (Linear Discriminant Analysis Effect Size) was used to analyze inter-group differences across taxonomic levels, selecting features with LDA > 3 and $P < 0.05$. Visualization was performed using cladograms and bar charts generated via the R package ggplot2 (version 3.2.0). Differential abundance analysis between groups was conducted using the metagenomeSeq package (version 1.38.0), and Manhattan plots were created for visualization (ggplot2 version 3.2.0). Taxonomic classification was performed with DIAMOND and the NR database, and species with differential abundance were identified via the Wilcoxon test. Functional annotations were made using KEGG.

LC–MS/MS

Samples were thawed and metabolites were extracted using 80% methanol. Liquid samples were mixed with precooled methanol, while solid samples were extracted with methanol, followed by centrifugation. Supernatants were dried, redissolved, and stored at −80 °C. QC samples were created by pooling 10 μL from each extraction. Metabolite analysis was conducted using an UltiMate 3000 UPLC system with an ACQUITY UPLC T3 column, and detection was done with a Q-Exactive mass spectrometer. Data were processed with XCMS and metabolites were identified by matching retention times and m/z values. Statistical analysis, including PLS-DA, was conducted in R, with significant metabolites selected based on $P < 0.05$ and fold change > 1.2. Functional analysis and network mapping were done using KEGG.

Single-cell RNA sequencing

Jejunum tissues were pre-washed with 1 × PBS on ice, cut into 0.5 mm^2 pieces, and washed again. The tissue fragments were digested with 0.35% collagenase IV, 2 mg/ml papain, and 120 U/ml DNase I at 37 °C for 20 min, then neutralized with PBS containing 10% fetal bovine serum. The cell suspension was filtered, centrifuged at 300 g for 5 min, and resuspended in 1 × PBS with 0.04% BSA. Erythrocytes were lysed, and dead cells were removed with Dead Cell Removal MicroBeads. The final suspension, adjusted to 700–1200 cells/μL, was checked for viability (> 85%) using trypan blue and counted. Cells were loaded into the 10 × Chromium chip using the 10X Genomics Single-Cell 3' kit to capture around 10,000 cells. cDNA amplification and library preparation were performed, and sequencing was done on an Illumina NovaSeq 6000 (paired-end, 150 bp) with 20,000 reads per cell. Data were processed with Cell Ranger and aligned to the Sscrofa Ensemble 11.1 genome. Seurat was used for analysis, and t-SNE was employed for data visualization.

Fp.OMVs labeling

The collected Fp.OMVs were adjusted to a concentration of 1 mg/ml. They were then incubated with DIL dye (1:1000, Beyotime, China) for 20 min at room temperature, in conditions avoiding light exposure. Afterward, the labeled OMVs were collected by ultracentrifugation and washed with PBS to remove unbound dye, a process repeated three times. Finally, the labeled Fp.OMVs were collected and stored at −80 °C.

SEM

Intestinal tissue samples were collected and immediately fixed in 2.5% glutaraldehyde at 4 °C for 24 h. After fixation, the samples were washed three times with 0.1 M phosphate buffer (pH 7.4) and post-fixed with 1% osmium tetroxide for 1 h at room temperature. The tissues were dehydrated through a graded series of ethanol (30%, 50%, 70%, 90%, and 100%), followed by critical point drying. The dried samples were mounted on aluminum stubs, sputter-coated with gold–palladium, and examined under a scanning electron microscope. Images were captured at various magnifications to analyze the surface morphology of the intestinal villi.

TEM

A 10 μl sample of Fp.OMVs was placed on a copper grid and allowed to settle for 1 min, with excess liquid removed using filter paper. The grid was stained with 10 μl uranyl acetate for 1 min, and excess stain was removed with filter paper. After air drying for several minutes at room temperature, the samples were imaged using a transmission electron microscope at 80 kV. For particle size analysis, the exosome sample was diluted to 30 μl, and instrument performance was tested with a standard sample. The exosome sample was then loaded, ensuring gradient dilution to prevent clogging, and analyzed to obtain particle size and concentration information.

In vivo imaging

Piglets were administered Fp.OMVs treated with DIL at a dose of 1 mg/kg. Fluorescent imaging was performed at 6, 12, 18, and 24 h post-administration using a NightOWL. FL system. At each time point, piglets were placed in the imaging system, and fluorescence images were captured to detect OD_{549}. Multiple views were obtained to ensure comprehensive data collection. The fluorescence intensity was measured across consistent regions of interest in the intestine for each time point. Data were analyzed to

quantify fluorescence intensity and monitor changes over time. Control samples were used to validate the specificity and accuracy of fluorescence detection, and the imaging system calibration was checked before each session.

Bacterial growth measurement

Limosilactobacillus reuteri, *Prevotellamassilia timonensis*, and *Faecalibacterium prausnitzii* were cultured in media with varying concentrations of Fp.OMVs (10, 50, and 100 μg/ml). The bacterial growth was monitored over 48 h by measuring optical density (OD_{600}) at intervals of 0, 6, 12, 18, 24, 30, 36, 42, and 48 h. Growth curves were generated to evaluate the effect of OMVs on bacterial growth, with control groups for comparison.

Bacterial-Fp.OMVs binding analysis

Limosilactobacillus reuteri, *Prevotellamassilia timonensis*, and *Faecalibacterium prausnitzii* were cultured in media containing high concentrations of Fp.OMVs (100 μg/ml) under strict light-avoidance conditions and collected after 6 h. In a light-avoidant environment, the bacteria were washed three times with PBS, fixed with 4% paraformaldehyde, washed again with PBS, and mixed with Anti-Fade Mounting Medium. The samples were then placed on slides and observed using a Nikon A1 (HD25) system. Additionally, the remaining bacteria from each group were analyzed for DIL-positive bacteria using the LSRFortessa™ system (BD) for flow cytometry analysis.

Flow cytometry

Vero and IPEC-J2 cells were cultured to 80% confluence and then switched to maintenance medium. The cells were pre-treated with various concentrations of PC (1, 5, and 10 μM), or with a combination of PC (10 μM) and inhibitors Necrostatin-1 (20 μM) and GSK-872 (5 μM) for 24 h. Following pre-treatment, the cells were infected with PEDV at a multiplicity of infection (MOI) of 0.1. After 24 h of infection, the cells were collected, washed twice with pre-cooled PBS, and centrifuged at 500 × g for 5 min at 4 °C. The cell concentration was adjusted to 5×10^6 cells/ml. Subsequently, 100 μl of the cell suspension was taken and incubated with 5 μl of Annexin V-APC and 5 μl of PI. The mixture was gently vortexed and incubated in the dark at room temperature for 10 min. Finally, 400 μl of pre-cooled PBS was added, and the samples were gently mixed. The stained cells were then analyzed using a flow cytometer (BD LSRFortessa). The data was analyzed by FlowJo 10.8.1 software.

Fecal PC concentration determination

According to the reagent manufacturer's instructions (elabscience, China), 1 g of feces was homogenized, centrifuged at 10,000 × g for 10 min at 4 °C, and the supernatant was taken to measure OD_{550}.

Cell viability assay

Vero and IPEC-J2 cells were seeded into 96-well plates (100 μl/well) and cultured until they reached 80% confluence. The cells were then treated with various concentrations of Phosphorylcholine (PC) (1, 5, 10, 20, 50, 100, 200, 500, 1000, 2000, and 5000 μM) for 24 h. After this period, 10 μl of CCK-8 solution was added to each well, and the plates were incubated for 2 h. Absorbance at 450 nm was measured using a microplate reader to evaluate the cytotoxicity of PC. Additionally, cells were pre-treated with 10 μM PC, either alone or in combination with the inhibitors Necrostatin-1 (20 μM) and GSK-872 (5 μM) (both from Medchemexpress, USA) for 24 h. This was followed by infection with PEDV at a multiplicity of infection (MOI) of 0.1. After 24 h of infection, cell viability was assessed using the CCK-8 method.

Western blot analysis

Animal Samples: Intestinal tissues were placed in ice-cold PBS, cut into 1–2 cm pieces, and digested with 0.25% trypsin–EDTA at 37 °C for 20 min. After washing, tissues were further digested with collagenase IV and DNase I at 37 °C for 30–60 min, filtered, and centrifuged.

Cell Line Samples: Vero and IPEC-J2 cells (80% confluence) were pre-treated with PC (1, 5, 10 μM) or Fp.OMVs (1, 5, 10 μg) for 24 h, followed by PEDV infection (MOI = 0.1). Cells were lysed with RIPA buffer, centrifuged, and protein concentration was measured using a BCA kit.

(See figure on next page.)

Fig. 1 *F.prausnitzii* alleviates intestinal viral infection in a piglet model. **a** Development of a functional model for *F.prausnitzii*; piglet small intestines were sampled on day 5 post-infection to assess intestinal damage, Fp + PEDV ($n = 8$), PEDV ($n = 8$), Control ($n = 5$). Comparative analysis of clinical indicators of survival (**b**), weight loss (**c**), and diarrhea (**d**) among the piglet groups. **e** Analysis of epithelial cell shedding from pathological sections. **f** Comparison of histopathological changes (H&E staining); images taken at 20 × and 100 × magnifications. **g** Alterations in intestinal appearance. **h** Scanning electron microscopy (SEM) examination of jejunal villi; images taken at 10 ×, 200 ×, and 500 × magnifications. **i** Assessment of relative PEDV-S expression levels in the intestines. **j** Immunofluorescence analysis of the intestines using PEDV-S; images taken at 100 × magnification. **k** Characterization of viral content in intestinal epithelial cells using PEDV-N. Results are shown as means ± SD, with statistical significance determined by t tests for two groups and one-way ANOVA for three groups. *$P < 0.05$; **$P < 0.01$; ****$P < 0.0001$. Panels **a** was created with BioRender.com

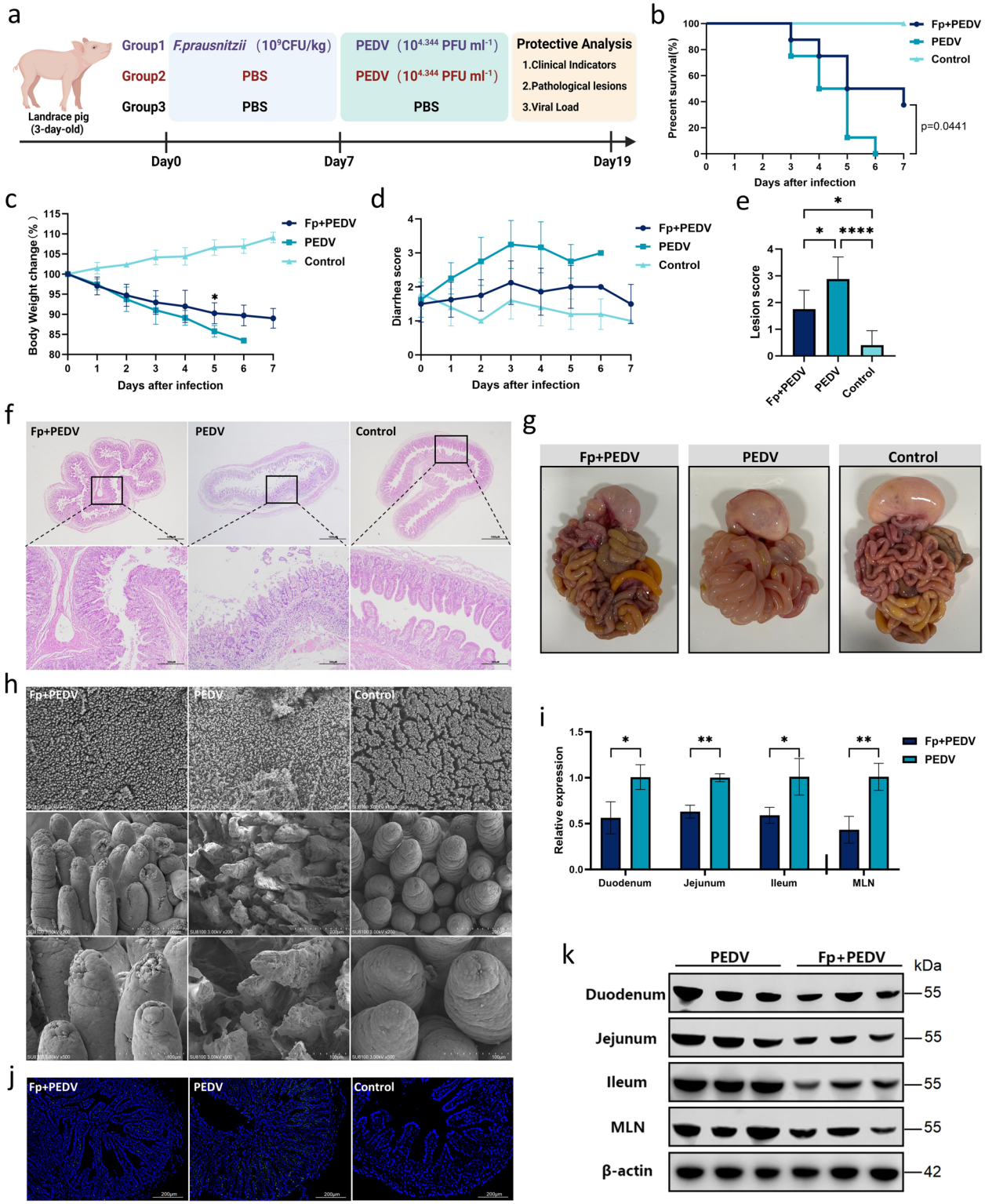

Fig. 1 (See legend on previous page.)

Proteins were separated by SDS-PAGE, transferred to PVDF membranes, and blocked. After blocking, membranes were incubated overnight at 4 °C with the following primary antibodies: PEDV-N (Medgene Labs, USA), RIPK1 (Proteintech, USA), P-RIPK1 (Proteintech, USA), RIPK3 (Proteintech, USA), P-RIPK3 (Nature Biosciences, China), MLKL (Proteintech, USA), P-MLKL (ABclonal, USA), β-actin (Proteintech, USA), and GAPDH (Proteintech, USA). After washing, secondary antibodies were applied, and proteins were visualized using ECL on the Amersham Imager 600.

Quantitative PCR

Following euthanasia, small intestine tissues were collected from piglets, and RNA was extracted using an RNA extraction kit (Takara, Japan) following the manufacturer's instructions. The extracted RNA was converted to cDNA using the SweScript RT II First Strand cDNA Synthesis Kit (Servicebio, China). Quantitative PCR was then performed using 2 × SYBR Green qPCR Master Mix (Servicebio, China) on a 7500 Real-Time PCR System. The primer sequences for PEDV-S were as follows: Forward: 5'-GTCAAGGAAATTGTCATCACCAAG-3' and Reverse: 5'-CAGCATCCAACAAACCGAGA-3'.

Histopathology and IFA assessment

On the 5th day post-PEDV infection, jejunum tissues from piglets were fixed in 4% paraformaldehyde and then embedded in paraffin. The tissues were dehydrated through a graded ethanol series and sectioned. For each sample, at least two 3-μm-thick sections were prepared and stained with hematoxylin and eosin (HE). The stained sections were analyzed using an inverted fluorescence microscope (Leica Microsystems, Germany). Another tissue section was stained with anti-PEDV-S antibody (1:1000) (LanDuBio, China), followed by incubation with FITC-conjugated goat anti-mouse antibody (1:1000) (Servicebio, China). The cells were then stained with DAPI for 5 min and covered with an anti-fade reagent (Beyotime, China). The sections were observed under a fluorescence microscope (Leica Microsystems, Germany) in a dark room, and images were captured at 200 × magnification.

Scoring for small intestinal changes was based on the grade of epithelial cell desquamation, measured as follows: 0 = normal (no desquamation), 1 = mild (a few desquamated cells of tip villous epithelium), 2 = moderate (desquamation of upper villous epithelium), 3 = marked (desquamation of lower villous epithelium), and 4 = severe (desquamation of crypt epithelium). Nine regions were randomly selected on the intestinal tissue sections to determine the average lesion change [29].

Statistical analysis

Metagenomic sequencing of piglet gut contents, untargeted metabolomic sequencing of bacterial culture supernatants and gut contents, and single-cell sequencing of piglet gut were performed and analyzed using the OmicStudio platform (www.omicstudio.cn). All data are expressed as the mean ± SD. Statistical analysis was performed using one-way ANOVA and t tests with GraphPad Prism 10.0 (GraphPad software). In the case of multiple comparisons, *P* values were corrected using Tukey's method. The *P* values are indicated as follows: $^{*}P < 0.05$; $^{**}P < 0.01$; $^{***}P < 0.001$; $^{****}P < 0.0001$.

Results

F.prausnitzii alleviates PEDV infection in a piglet model

We utilized a piglet infection model with PEDV, known for its stable infection in piglets, to examine the role of *F.prausnitzii*. Three-day-old Landrace piglets were randomly assigned to three groups. On day 7, 16 piglets were infected with PEDV, followed by a 7-day analysis of clinical indicators, pathological damage, and viral load detection (Fig. 1a). The findings indicated that the survival rate of the Fp + PEDV group was significantly higher than that of the PEDV group post-infection ($P = 0.0441$) (Fig. 1b). The Fp + PEDV group experienced less weight loss and maintained a higher body weight percentage compared to the PEDV group, suggesting a beneficial effect of

(See figure on next page.)

Fig. 2 Fp.OMVs play a key role in alleviating intestinal viral infection. **a** Creation of a screening model for *F.prausnitzii* functional substances; piglet small intestines were sampled on day 5 post-infection to assess intestinal damage. Groups included Fp.supernatant + PEDV ($n = 6$), Fp.inactivated + PEDV ($n = 6$), Fp.OMVs + PEDV ($n = 6$), PEDV ($n = 6$), and Control ($n = 6$). Comparative analysis of clinical indicators of survival (**b**), weight loss (**d**), and diarrhea (**e**) in each piglet group. **c** Analysis of the digestive kinetics of DIL-labeled Fp.OMVs in piglet intestines using an in vivo imaging system; fluorescence signals were collected at 6, 12, 18, and 24 h. **f** Scanning electron microscopy analysis of jejunal villi; images taken at 10 ×, 200 ×, and 500 × magnifications. **g** Alterations in intestinal appearance. **h** Comparison of histopathological changes (H&E staining); images taken at 20 × and 100 × magnifications. **i** Characterization of viral content in intestinal epithelial cells using PEDV-N. **j** Immunofluorescence analysis of the intestines using PEDV-S; images taken at 100 × magnification. **k** Assessment of relative PEDV expression levels in the intestines. **l** Analysis of epithelial cell shedding from pathological sections. Results are presented as means ± SD, with statistical significance determined by t tests for two groups and one-way ANOVA for four and five groups. $^{*}P < 0.05$; $^{**}P < 0.01$; $^{***}P < 0.001$; $^{****}P < 0.0001$. Panel **a** was created with BioRender.com

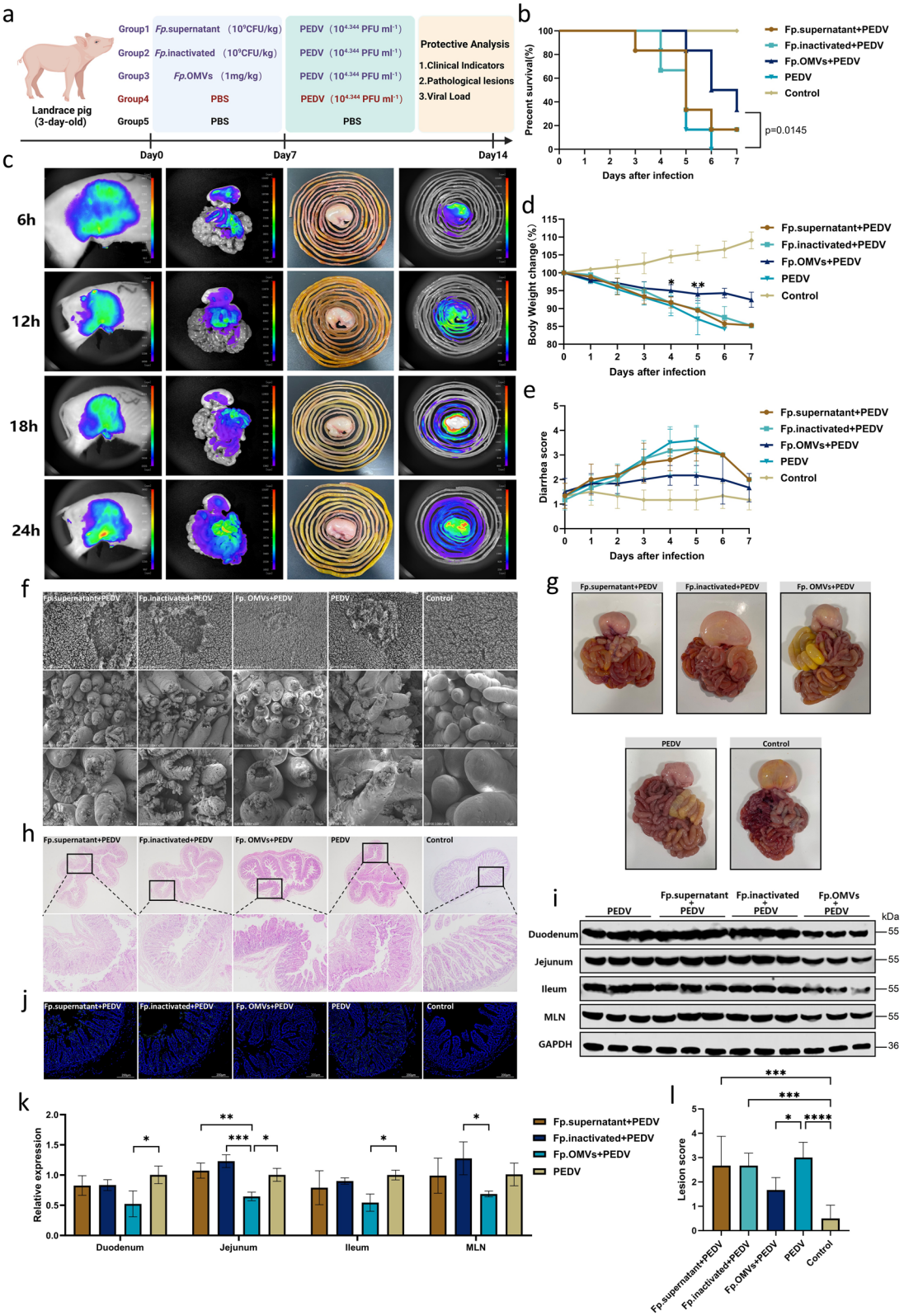

Fig. 2 (See legend on previous page.)

F.prausnitzii on weight maintenance (Fig. 1c). Additionally, the Fp + PEDV group exhibited milder and shorter diarrhea symptoms (Fig. 1d). Further examination, including lesion scoring using HE staining (Fig. 1e, f) and intestinal appearance analysis (Fig. 1g), revealed that the Fp + PEDV group had more intact intestinal villi and healthier intestinal tissue structures, whereas the PEDV group displayed severe villous damage and significant tissue destruction. These findings were further confirmed by scanning electron microscopy results (Fig. 1h). qPCR analysis revealed significantly lower viral replication levels in various intestinal segments and mesenteric lymph nodes in the Fp + PEDV group (Duodenum, $P = 0.0255$; Jejunum, $P = 0.0015$; Ileum, $P = 0.0287$; MLN, $P = 0.0086$) (Fig. 1i), with viral replication quantified by measuring the PEDV-S expression. Immunofluorescence staining (Fig. 1j) and Western blot (Fig. 1k) confirmed a reduction in PEDV antigen and viral protein expression in the intestines of the Fp + PEDV group.

Fp.OMVs play a key role in alleviating viral infection

Bacteria can influence immunity and infection through surface proteins, metabolites, and OMVs [29, 31–33]. To identify the active substances by which *F.prausnitzii* exerts its effects, we isolated its culture supernatant, OMVs, and inactivated bacteria for functional analysis. On day 7, the piglets were infected with PEDV, followed by a 7-day functional evaluation (Fig. 2a). To confirm whether Fp.OMVs can effectively enter the gut, we labeled them with $DILC_{18}(3)$ (DIL) and monitored their digestive kinetics at 6, 12, 18, and 24 h. The results indicated that the OMVs diffused and were digested over time, starting from the stomach and duodenum at 6 h and accumulating in the ileum by 24 h (Fig. 2c). The results showed that the survival rate of the Fp.OMVs + PEDV group was significantly higher than that of the PEDV group ($P = 0.0145$) (Fig. 2b). The Fp.OMVs + PEDV group experienced the least weight loss, maintaining over 90% of their body weight throughout the study (Fig. 2d), and exhibited milder diarrhea symptoms (Fig. 2e). Scanning electron microscopy (Fig. 2f) and HE staining (Fig. 2h) revealed that the intestinal villi and tissue structure of the Fp.OMVs + PEDV group were the most intact, while the other treatment groups and the PEDV group showed varying degrees of damage and extensive shedding of intestinal epithelial cells. In terms of overall gut health, the Fp.OMVs + PEDV group displayed a healthy state, while the other treatment groups and the PEDV group exhibited clear lesions such as congestion and edema (Fig. 2g). Immunofluorescence staining (Fig. 2j) and Western blot (Fig. 2i) results confirmed that pretreatment with OMVs reduced the expression of viral antigens and proteins. qPCR analysis demonstrated that the viral replication levels in various intestinal segments and mesenteric lymph nodes were lower in the Fp.OMVs + PEDV group compared to the other treatment groups and the PEDV group (Fig. 2k). Finally, lesion scoring showed that the Fp.OMVs + PEDV group had significantly lower scores than the other treatment groups and the PEDV group (Fig. 2l).

Characterization of proteins, small RNAs, and metabolites in Fp.OMVs

To date, a comprehensive analysis of the structure and composition of Fp.OMVs has not been performed. We collected OMVs using concentration and ultracentrifugation methods (Fig. 3a). Transmission electron microscopy revealed that the diameter of Fp.OMVs ranges from approximately 30–150 nm, and they are round in shape (Fig. 3b, Fig. S1a, b). Next, we employed sequencing techniques to analyze the proteins, metabolites, and small RNAs in the OMVs (Fig. 3c). At the protein level, we identified a total of 1,326 proteins, including Pgsa, Rplt, Rpsl, Rpll, Grol, Crt, Etfa, and Rpsd, which are highly expressed and functional within bacterial cells. Subcellular localization analysis showed that the main components were cytoplasm proteins and cell inner membrane proteins, accounting for 45.24% and 41.99%, respectively, with the remaining being periplasm proteins (9.52%), extracellular proteins (2.60%), and cell outer membrane proteins (0.65%) (Fig. 3d). Functional enrichment comparison using IPR, GO, COGs, and KEGG databases revealed 696 common genes (Fig. 3e). IPR functional annotation indicated that ABC transporter-like functions were the most abundant among proteins identified in the OMVs (Fig. S1c). Additionally, we identified 352 and 180 metabolites under positive and negative ion

(See figure on next page.)

Fig. 3 Characterization and composition analysis of Fp.OMVs. **a** Process for collecting Fp.OMVs. **b** Analysis of Fp.OMVs using transmission electron microscopy. **c** Detection of proteins, metabolites, and miRNAs in Fp.OMVs using proteomics, untargeted metabolomics, and small RNA-Seq. Structures of proteins and miRNAs were generated with AlphaFold3, while metabolite structures were generated with ChemDraw and presented as an exploded view of Fp.OMVs. **d** Subcellular localization analysis of Fp.OMVs proteins based on Cell-mPLOC. **e** Functional analysis of Fp.OMVs proteins based on IPR, GO, COGs, and KEGG databases. Classification and proportion of Fp.OMVs metabolic components under positive ion (**f**) and negative ion (**g**) modes. Panel **a** was created with BioRender.com

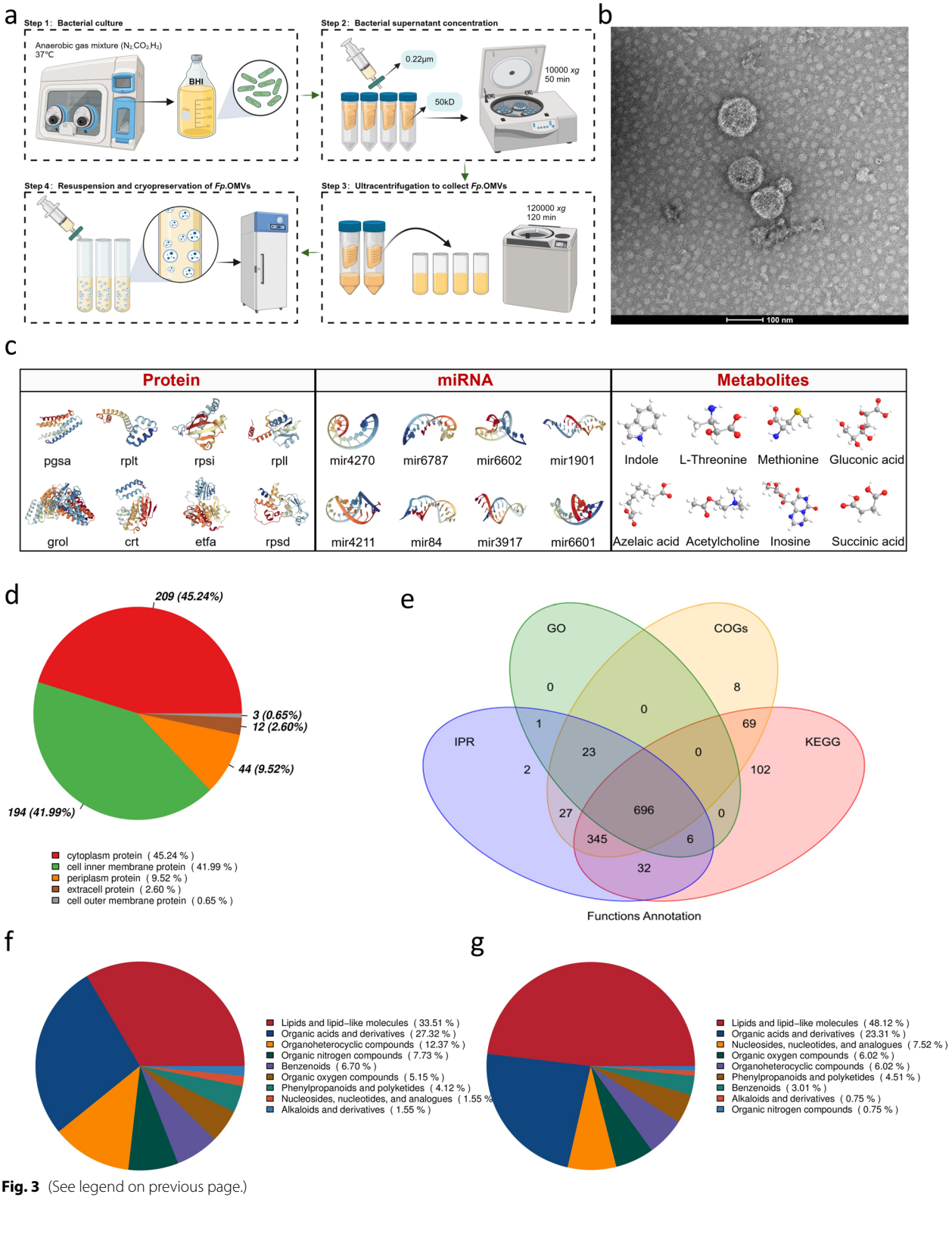

Fig. 3 (See legend on previous page.)

modes, respectively (Fig. 3f, g). Major components included Indole, L-Threonine, Methionine, Gluconic acid, Azelaic acid, Acetylcholine, Inosine, and Succinic acid. Lipids and lipid-like molecules, as well as organic acids and derivatives, were the predominant categories in both ion modes. Comparison with the HMDB database showed successful identification of 44 and 45 metabolites in the Lipids and lipid-like molecules and Organic acids and derivatives categories, respectively (Fig. S1d). Finally, we analyzed small RNAs, which had sequence lengths ranging from 17 to 150 nucleotides, with the highest number of sequences being 1,696,222 at a length of 22 nucleotides. These small RNAs were classified into various types, including miRNA, Cis-regulatory RNA, lncRNA, rRNA, snoRNA, and snRNA. Different families of miRNA were identified, with total lengths ranging from 16 to 32 nucleotides, such as mir4270, mir6787, mir6602, mir1901, mir4211, mir84, mir3917, and mir6601 (Fig. S1e).

Fp.OMVs rely on gut microbiota to alleviate viral infection

The exact mechanism by which Fp.OMVs function is still unclear. We pretreated Vero and IPEC-J2 cells with a safe concentration of Fp.OMVs (Fig. S2a, b) before infecting them with PEDV. The results indicated that direct application of Fp.OMVs did not reduce the viral load (Fig. S2c, d), suggesting an indirect mechanism of action. Bacteria use OMVs to exchange information, impacting microbial community niches and metabolic functions [34, 35]. To investigate whether the function of Fp.OMVs depends on the gut microbiota, we established a piglet gut microbiota disruption model using antibiotic treatment (Fig. 4a). We found that, compared to the Fp.OMVs + PEDV group, the Abx + Fp.OMVs + PEDV group had a similar survival rate to the PEDV group, negating the protective effect of Fp.OMVs (Fig. 4b). Weight change data showed accelerated weight loss in the Abx + Fp.OMVs + PEDV group (Fig. 4c) and a significant increase in diarrhea scores (Fig. 4f), indicating that Fp.OMVs lost their protective effect in the absence of a normal gut microbiota. Scanning electron microscopy (Fig. 4e) and HE staining (Fig. 4g) further supported this conclusion, showing severe damage to the intestinal villi structure in the Abx + Fp.OMVs + PEDV group, compared to milder damage in the Fp.OMVs + PEDV group. Lesion scores between the Abx + Fp.OMVs + PEDV and PEDV groups showed no significant difference (Fig. 4d). Additionally, gross intestinal examination revealed obvious lesions in the Abx + Fp.OMVs + PEDV group, while the Fp.OMVs + PEDV group maintained relatively mild edema (Fig. 4h). Immunofluorescence staining (Fig. 4i) and Western blot (Fig. 4k) results showed a similar trend, with increased viral protein expression in the Abx + Fp.OMVs + PEDV group. We also observed that viral replication levels in various intestinal segments and mesenteric lymph nodes were higher in the Abx + Fp.OMVs + PEDV group compared to the Fp.OMVs + PEDV group (Fig. 4j). In summary, the function of Fp.OMVs largely depends on the presence of the gut microbiota. Depletion of the gut microbiota abolishes the mitigating effects of Fp.OMVs on viral infection.

Fp.OMVs alter the structure and abundance of the gut microbiota and stimulate bacterial growth in vitro

To identify which bacterial categories are affected by Fp.OMVs, we employed metagenomic methods to analyze the impact of OMVs on the gut bacterial community. The Shannon Index (Fig. S3a), Observed Species (Fig. S3b), and Chao1 (Fig. S3c) metrics revealed the richness and evenness of gut microbiota under different treatment conditions. The shared Unigenes between the Fp.OMVs + PEDV group and the PEDV group totaled 2,289,768, while the Fp.OMVs + PEDV group had 40,697 unique Unigenes (Fig. S3d). Alpha diversity analysis showed that the Simpson index, Goods coverage, Shannon index, and observed species count in the Fp.OMVs + PEDV group were significantly higher than in the PEDV group (Fig. 5a). Beta diversity analysis using PCA (Fig. 5b), PCoA (Fig. S3e), NMDS (Fig. S3f) and PERMANOVA ($P < 0.0001$) (Supplementary information Table 1) demonstrated that Fp.OMVs significantly altered the microbial structure in the piglet gut. Relative

(See figure on next page.)

Fig. 4 Fp.OMVs function depends on the gut microbiota. **a** Creation of a piglet intestinal microbiota depletion model; piglet small intestines were collected on day 5 post-infection to evaluate intestinal damage in groups Abx + Fp.OMVs + PEDV ($n = 6$), Fp.OMVs + PEDV ($n = 6$), PEDV ($n = 6$), and Control ($n = 6$). Comparative analysis of survival (**b**), weight loss (**c**), and diarrhea (**f**) in each piglet group. **d** Analysis of epithelial cell shedding from pathological sections. **e** Scanning electron microscopy analysis of jejunal villi; images taken at 10×, 200×, and 500× magnifications. **g** Comparison of histopathological changes (H&E staining); images taken at 20× and 100× magnifications. **h** Alterations in the appearance of the intestines. **i** Immunofluorescence analysis of the intestines using PEDV-S; images taken at 100× magnification. **j** Assessment of relative PEDV expression levels in the intestines. **k** Characterization of viral content in intestinal epithelial cells using PEDV-N. Results are presented as means ± SD, with statistical significance determined by t tests for two groups and one-way ANOVA for three and four groups. *$P < 0.05$; **$P < 0.01$; ****$P < 0.0001$. Panel **a** was created with BioRender.com

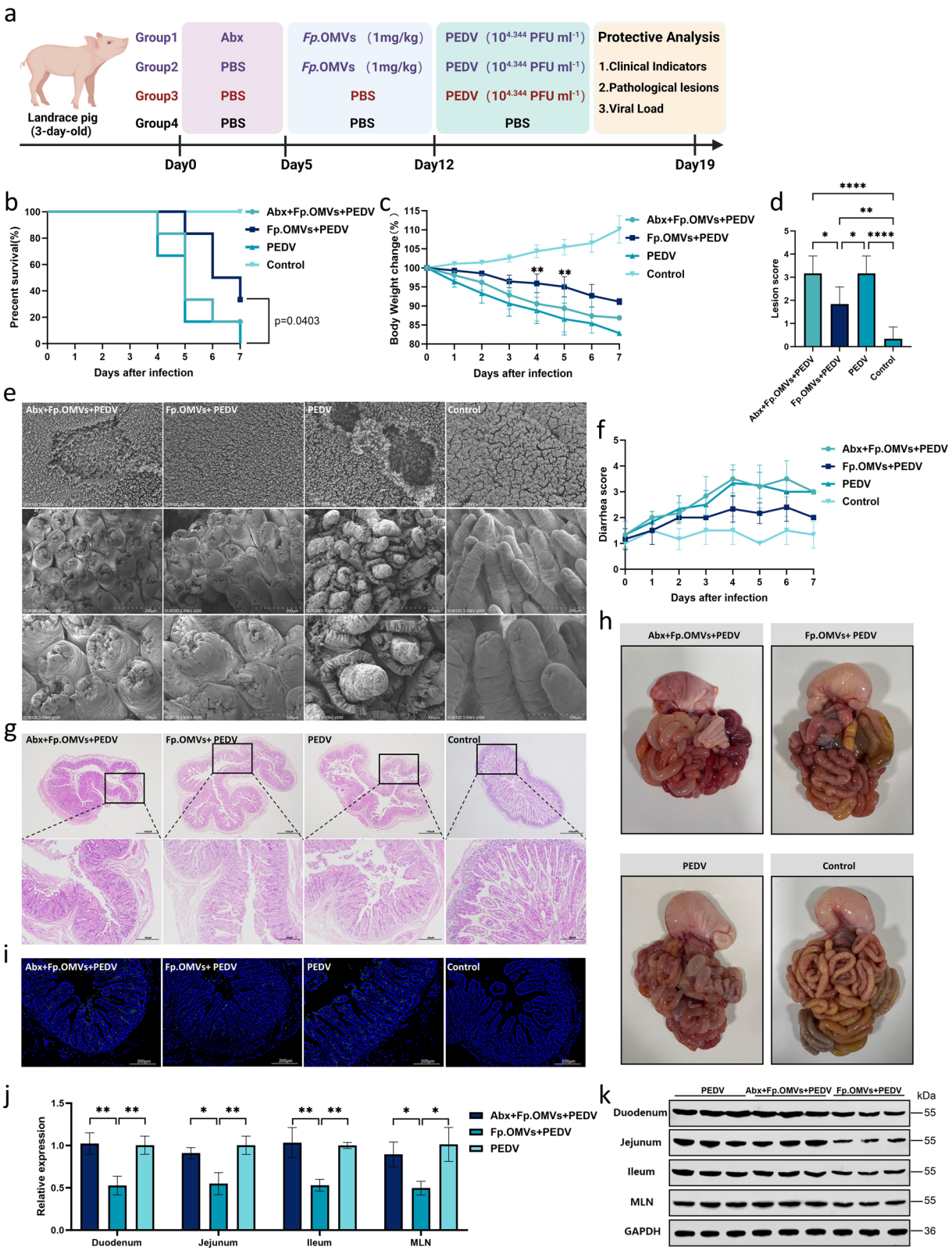

Fig. 4 (See legend on previous page.)

abundance analysis at the phylum (Fig. S3g), genus (Fig. S3h), and species levels (Fig. 5c) revealed significant increases in the abundances of *Euryarchaeota* and *Pseudomonadota* at the phylum level in the Fp.OMVs + PEDV group. At the genus level, the abundances of *Prevotella*, *Faecalibacterium*, and *Lactobacillus* were significantly increased in the Fp.OMVs + PEDV group, with notable upregulation of species such as *Prevotella* sp. P5-92, *Segatella copri*, *Faecalibacterium prausnitzii*, and *Lactobacillus johnsonii*. LEfSe analysis supported these findings, showing high-expression communities of genera like *Prevotella*, *Faecalibacterium*, and *Lactobacillus*, and species such as *Faecalibacterium prausnitzii*, *Prevotellamassilia timonensis*, and *Limosilactobacillus reuteri* in the Fp.OMVs + PEDV group (Fig. 5d, e, f and Fig. S3i). Bacterial OMVs facilitate interspecies communication and community signaling. We hypothesized that Fp.OMVs could bind to or enter other bacteria to influence their growth. To test this, we pre-labeled OMVs with DIL and co-cultured them with *Limosilactobacillus reuteri*, *Prevotellamassilia timonensis*, and *Faecalibacterium prausnitzii*. Confocal microscopy showed that Fp.OMVs could bind to all three bacterial species (Fig. 5g). In vivo abundance alone does not fully capture the impact of OMVs on bacteria. Therefore, we cultured the three upregulated bacteria with different concentrations of Fp.OMVs in vitro. Interestingly, Fp.OMVs (10, 50, and 100 μg/ml) stimulated the growth of *Limosilactobacillus reuteri* (Fig. 5h), *Prevotellamassilia timonensis* (Fig. 5i), and *Faecalibacterium prausnitzii* (Fig. 5j), including self-growth stimulation of *Faecalibacterium prausnitzii*. This binding was further confirmed by flow cytometry, which demonstrated a increase in DIL^+ *Limosilactobacillus reuteri* (Fig. 5l, m, k), DIL^+ *Prevotellamassilia timonensis* (Fig. 5o, p, n), and DIL^+ *Faecalibacterium prausnitzii* (Fig. 5r, s, q) after treatment with Fp.OMVs. In conclusion, Fp.OMVs alter the composition and abundance of the gut microbiota in vivo, a phenomenon also observed in vitro.

Fp.OMVs modulate the metabolic profiles of the intestine and associated bacteria

Metabolites were quantified using untargeted metabolomics via LC–MS/MS, and the abundance of each metabolite was normalized to the total ion current for statistical comparison. Besides impacting bacterial growth, Fp.OMVs are likely to alter bacterial functions. KEGG analysis indicated notable changes in the genes related to bacterial metabolic pathways in the gut (Fig. S3j). We identified the upregulated metabolites following Fp.OMVs treatment, noting that Glycerophospholipids, Fatty Acyls, Carboxylic acids and derivatives, and Prenol lipids were the primary categories in both bacterial cultures of *Limosilactobacillus reuteri* (Fig. 6a), *Prevotellamassilia timonensis* (Fig. 6c), *Faecalibacterium prausnitzii* (Fig. 6d), and the intestinal environment (Fig. 6e). Further analysis of the next level of metabolites showed that Fp.OMVs treatment increased key substances downstream of Glycerophospholipids, such as PC, PA, and PG, with a significant rise in PC. Additionally, there were substantial increases in Arachidonic acid, FAHFA36:3, Tomentosic acid, Maslinic Acid, Euscaphic acid, and b-Boswellic acid within the Fatty Acyls and Prenol lipids categories (Fig. 6b). Differential analysis of the metabolites indicated that PC-group metabolites like PC(DiMe(11,3)/6keto-PGFialpha), PC(18:4(62,92.122.15Z)/6 keto-PGF1alpha), PC(16:0/PGE1), PC(15:0/20:4(6Z,8E,10E,14Z)−2OH(5S,12R)), PC(15:0/0:0), and PC O-17:0 were significantly upregulated in both bacterial cultures of *Limosilactobacillus reuteri* (Fig. 6f), *Prevotellamassilia timonensis* (Fig. 6g), *Faecalibacterium prausnitzii* (Fig. 6h), and the intestinal environment (Fig. 6i). Following this, we investigated the metabolic variations induced by Fp.OMVs in the intestinal environment and during in vitro co-cultures with *Limosilactobacillus reuteri*, *Prevotellamassilia timonensis*, and *Faecalibacterium prausnitzii*. PLS-DA analysis revealed that Fp.OMVs modified the metabolic profiles of *Limosilactobacillus reuteri* (Fig. 6j), *Prevotellamassilia*

(See figure on next page.)

Fig. 5 Fp.OMVs bind to specific bacteria and stimulate their growth. **a** Comparative analysis of Simpson index, Goods coverage index, Shannon index, and observed species index between the Fp.OMVs + PEDV ($n = 15$) and PEDV ($n = 15$) groups. **b** PCA analysis based on weighted UniFrac distances to identify microbial structural changes. **c** Top 20 species at the species level between the Fp.OMVs + PEDV and PEDV groups. **d** LEfSe-based differential species abundance analysis (*Faecalibacterium prausnitzii*, *Prevotellamassilia timonensis*, and *Limosilactobacillus reuteri*). **e** Bacterial phylogenetic branches, with different circle layers from inner to outer representing seven taxonomic levels: domain, phylum, class, order, family, genus, and species; each node represents a species classification at that level. **f** LEfSe analysis (LDA score > 3). **g** Co-localization results of DIL-labeled Fp.OMVs with *Limosilactobacillus reuteri*, *Prevotellamassilia timonensis*, and *Faecalibacterium prausnitzii* detected by laser confocal microscopy. Growth measurements of *Limosilactobacillus reuteri* (**h**) ($n = 3$), *Prevotellamassilia timonensis* (**i**) ($n = 3$), and *Faecalibacterium prausnitzii* (**j**) ($n = 3$) pre-treated with different concentrations of Fp.OMVs, Fp.OMVs-L, 10 μg/mL; Fp.OMVs-M, 50; Fp.OMVs-H, 100 μg/mL. Flow cytometry combined analysis of DIL-labeled Fp.OMVs with *Limosilactobacillus reuteri* (**l**, **m**, **k**), *Prevotellamassilia timonensis* (**o**, **p**, **n**), and *Faecalibacterium prausnitzii* (**r**, **s**, **q**); results presented using scatter plots, statistical charts, and histograms. Results are presented as means ± SD, with statistical significance calculated by t tests for two groups and one-way ANOVA for four groups. $^{**}P < 0.01$; $^{***}P < 0.001$; $^{****}P < 0.0001$

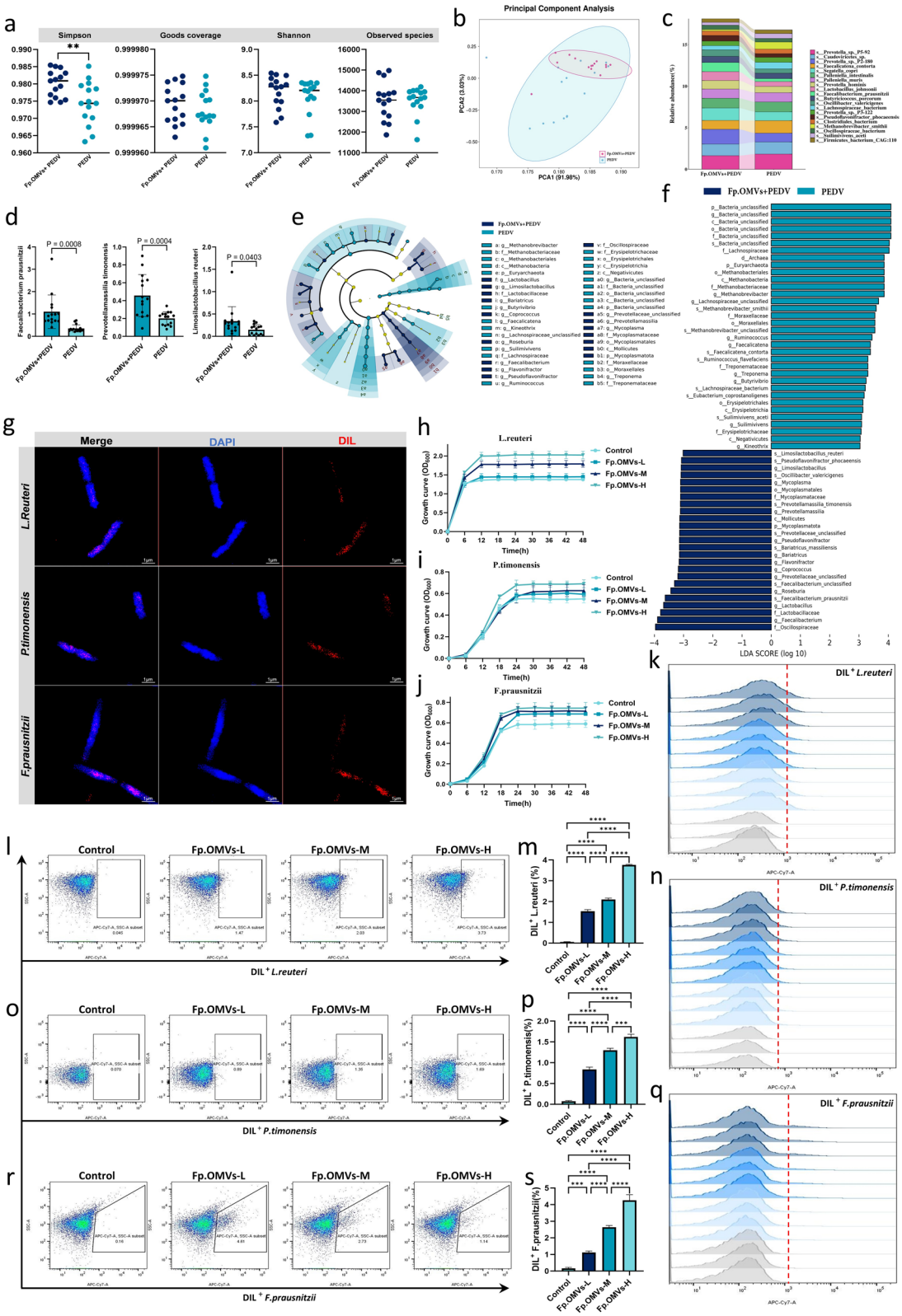

Fig. 5 (See legend on previous page.)

timonensis (Fig. 6k), *Faecalibacterium prausnitzii* (Fig. 6l), and the intestinal environment (Fig. 6m). Finally, gene function prediction on the metabolites in *Limosilactobacillus reuteri* (Fig. 6n), *Prevotellamassilia timonensis* (Fig. 6o), *Faecalibacterium prausnitzii* (Fig. 6p), and the intestinal environment (Fig. 6q) post-Fp.OMVs treatment showed enrichment in functions related to Cellular Processes, Metabolism, and Organismal Systems. In conclusion, Fp.OMVs not only significantly alter the metabolic composition of the piglet gut but also affect the metabolic activities of specific bacteria.

Gut microbiota-derived PC alleviates viral infection

Our differential metabolomics analysis revealed a enrichment of PC-like substances following Fp.OMVs treatment. These metabolites, mostly precursors or intermediates of PC, led us to hypothesize that PC might play a functional role during viral infection. The measurement of PC in piglet intestinal feces revealed that Fp.OMVs significantly increased the PC content in vivo ($P=0.0089$) (Fig. 7a). We established a piglet viral infection model, using antibiotic treatment to eliminate interference from metabolites produced by other microorganisms (Fig. 7b). The results indicated that PC mitigated the negative impacts of the virus, as evidenced by improved survival rates (Fig. 7c) and body weight changes (Fig. 7d) compared to the PEDV group. In addition, PC alleviated broken villi and extensive epithelial cell shedding, consistent with the pathology scoring results (Fig. 7e). The diarrhea index also showed improvement (Fig. 7g), maintaining a stable trend from day 4 to day 7. Scanning electron microscopy (Fig. 7f) and HE staining (Fig. 7i) revealed that the intestinal villi and tissue structure of the PC pretreatment group remained intact, with only mild damage and epithelial cell shedding. Additionally, the PC pretreatment group exhibited mild congestion and edema in gut appearance, while the PEDV group showed obvious lesions and severe congestion and edema (Fig. 7h). Viral load analysis demonstrated that the PC pretreatment group had lower viral replication levels in various intestinal segments and mesenteric lymph nodes compared to the PEDV group (Fig. 7j). Western blot results (Fig. 7k) and Immunofluorescence staining (Fig. 7l) also confirmed that PC could reduce viral load in different areas.

PC significantly alters intestinal cell subpopulation distribution under viral infection

The gut, a crucial immune organ, has its mucosal surface populated with numerous immune cells. Microbiota-produced metabolites stimulate the immune system to defend against intestinal pathogens [23, 36–38]. To understand how PC regulates viral infection, we analyzed cell distribution in the piglet gut using single-cell sequencing. These subpopulations were displayed in different groups using t-SNE (Fig. 8a). Further cell marker analysis identified 15 cell types, including T cells (CD3E, CD3D, CD4, CD8A, CD8B), B cells (CD19, MS4A1, CD79A, CD79B), Macrophages (CD163, CD68, CSF1R), Dendritic cells (CCR7, CD83, CD86, FSCN1), Monocytes (ITGAM, TYROBP, MYD88), Epithelial cells (EPCAM, VIL1, CLDN4, CLDN7, KRT8, KRT18), Goblet cells (MUC2, TFF3, SPDEF), Smooth muscle cells (TAGLN, ACTA2, CALD1), Endothelial cells (CLDN5, PECAM1, RAMP2), Enteroendocrine cells (CHGA, CHGB, PCSK1, GCG), Intestinal stem cells (OLFM4, REG4, TOP2A), Fibroblasts (DCN, COL1A1, COL1A2), MMPhigh-Fibroblasts (MMP1, MMP2, MMP3), Intestinal neurons (NCAM1, CADM1, PHOX2B), and Intestinal proliferative cells (AURKB, CDC20, PLK1) (Fig. 8b). To better visualize the subpopulation boundaries and cell morphology, we generated a gene marker map (Fig. 8c) and revealed the proportion of these subpopulations in the PC + PEDV and PEDV groups. We dissociated the entire jejunal tissue to create a comprehensive single-cell atlas. Based on differential gene sets, we identified 0–26 cell subpopulations, each expressing specific genes, such as PECAM1 and CLDN5 in subpopulation 0 (Fig. 8d). Cell abundance analysis showed that PC pretreatment increased the relative abundance of epithelial cells while reducing the relative abundance of T cells and B cells, which are critical for adaptive immunity (Fig. 8e). We then identified highly expressed genes in the early stage,

(See figure on next page.)

Fig. 6 Fp.OMVs alter the metabolic profiles of intestines and cultured bacteria, increasing PC class metabolites. Statistical analysis of differentially upregulated metabolite classes in *Limosilactobacillus reuteri* (Fp.OMVs group, $n=5$; Control group, $n=5$) (**a**), *Prevotellamassilia timonensis* (Fp.OMVs group, $n=5$; Control group, $n=5$) (**c**), and *Faecalibacterium prausnitzii* (Fp.OMVs group, $n=5$; Control group, $n=5$) (**d**) during in vitro culture, as well as in piglet intestines (Fp.OMVs + PEDV group, $n=15$; PEDV group, $n=15$) (**e**). **b** Statistical analysis of the number of downstream products of the top three classes of metabolites in different systems treated with Fp.OMVs. Volcano plot analysis of differentially abundant metabolites in *Limosilactobacillus reuteri* (**f**), *Prevotellamassilia timonensis* (**g**), *Faecalibacterium prausnitzii* (**h**), and piglet intestines (**i**) after Fp.OMVs pre-treatment. Partial least squares discrimination analysis (PLS-DA) of metabolites in *Limosilactobacillus reuteri* (**j**), *Prevotellamassilia timonensis* (**k**), *Faecalibacterium prausnitzii* (**l**), and piglet intestines (**m**) after Fp.OMVs pre-treatment. Functional comparative analysis of metabolic components in the KEGG database in *Limosilactobacillus reuteri* (**n**), *Prevotellamassilia timonensis* (**o**), *Faecalibacterium prausnitzii* (**p**), and piglet intestines (**q**) after Fp.OMVs pre-treatment

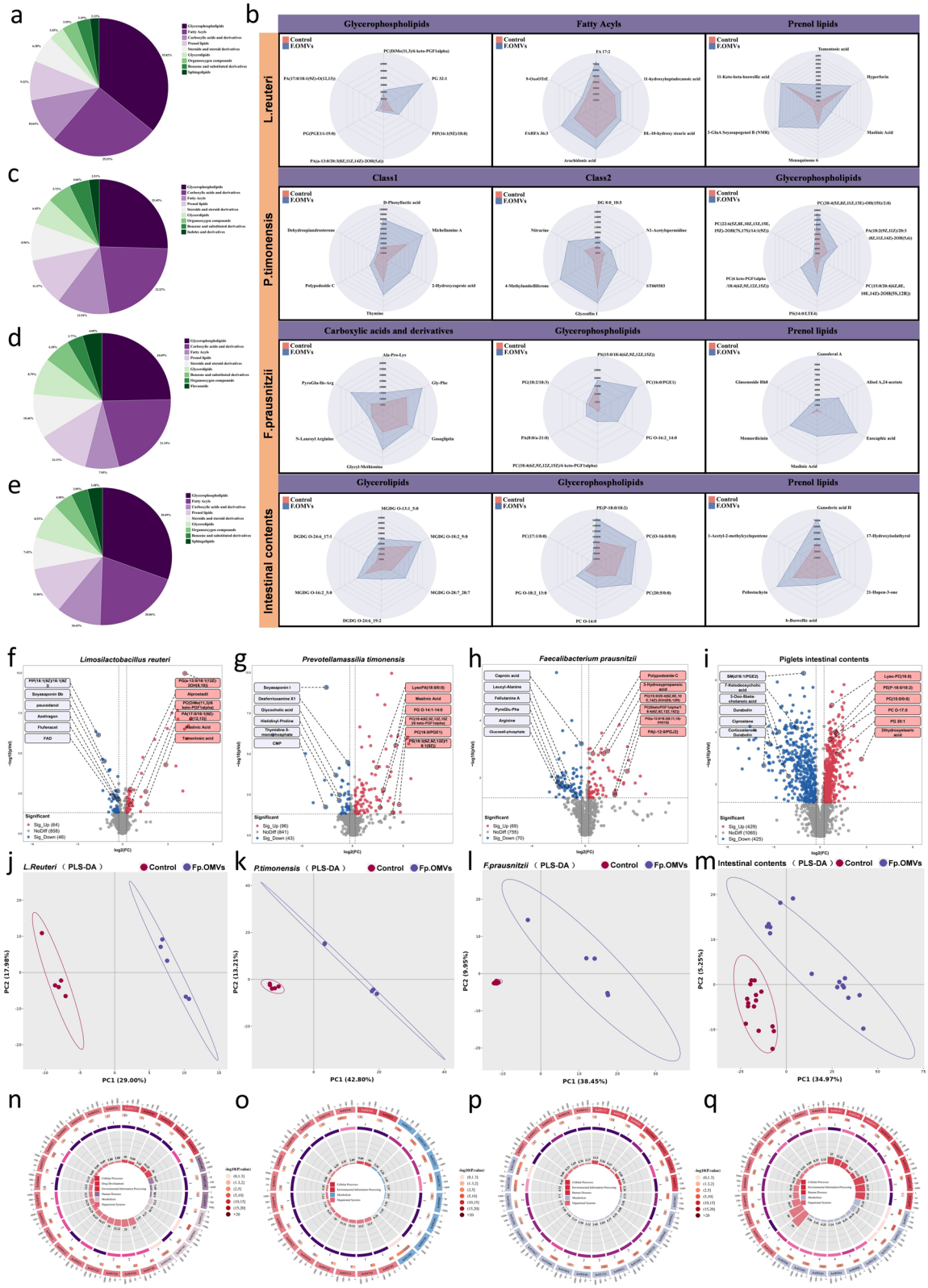

Fig. 6 (See legend on previous page.)

such as *RAB11A*, *STOM*, *LRRC19*, *ENPP3*, and *SLC51B*, as well as in the late stage, such as *BMP4*, *FERMT2*, *GJA1*, *NID2*, and *ANXA1* (Fig. 8f). In summary, PC pretreatment altered the distribution of intestinal cells under viral infection, predominantly rescuing a large number of epithelial cells.

PC reduces necroptosis induced by PEDV infection

Intestinal epithelial cells, due to their extensive exposure surface, are prone to viral contact and act as vectors for viral replication and transmission [39]. KEGG functional predictions of epithelial cells from PC-treated and control groups revealed that PC treatment reduced the expression of genes involved in the necroptosis pathway, indicating that PC may inhibit necroptosis during infection (Fig. 9a). To determine cytotoxicity, we treated two cell lines capable of PEDV infection, IPEC-J2 and Vero cells, with varying concentrations of PC (Fig. 9b, c). Concentrations of 1, 5, and 10 μM were used as low, medium, and high doses. After treatment, cells were infected with PEDV at MOI = 0.1 and harvested 24 h later. Flow cytometry was used to detect cell death, characterized in the Q2 quadrant. PC treatment at different concentrations inhibited PEDV-induced cell death in both IPEC-J2 and Vero cells (Fig. 9d, e, f). We also treated cells with the RIPK1 inhibitor Nec-1 and the RIPK3 inhibitor GSK-872 in combination with PC, further reducing cell death. This indicated that PC inhibited necroptosis-induced cell death during viral infection (Fig. 9g, h, i). RIPK1 interacts with RIPK3 to form the RIPK1-RIPK3 complex, which activates RIPK3 to phosphorylate MLKL. Phosphorylated MLKL accumulates at the cell membrane, forming pores that ultimately lead to cell death. We analyzed the phosphorylation levels of RIPK1, RIPK3, and MLKL in IPEC-J2 (Fig. 9j) and Vero cells (Fig. 9k) treated with different concentrations of PC. Compared to the PEDV infection group, PC treatment reduced the phosphorylation levels of RIPK1, RIPK3, and MLKL. Similarly, cell viability of IPEC-J2 (Fig. 9l) and Vero cells (Fig. 9m) treated with PC (10 μM) alone and in combination with inhibitors showed the same trend, indicating that PC reduces necroptosis induced by viral infection.

Discussion

Our study reveals the potential functions of *F.prausnitzii* and its OMVs in PEDV infection. Although *F.prausnitzii* is known for its anti-inflammatory properties and role in maintaining intestinal health, this study using a piglet model found that *F.prausnitzii* significantly reduced viral load and mitigated disease progression during viral infection. This discovery highlights the important role of the commensal bacterium *F.prausnitzii* in maintaining intestinal health and resisting pathogen invasion. Our study provides new insights into the prevention and treatment of PEDV.

Pigs were chosen for our study due to their anatomical, physiological, and genetic similarities to humans, making them superior disease models in biomedical research [40, 41]. OMVs, as mediators of intercellular communication, carry various bioactive substances that regulate host immune responses and microbiota structure [15, 34]. Functional analysis of *F.prausnitzii* culture supernatants, inactivated bacteria, and OMVs showed that only OMVs played a significant role in antiviral activity, improving clinical outcomes, reducing pathological damage, and lowering viral load. Bacterial OMVs, similar in size to mammalian EVs, are believed to mediate communication between bacteria and the host by transporting bioactive molecules, including proteins, nucleic acids, lipids, and metabolites, thus contributing to health or causing pathology [35]. We observed that Fp.OMVs could alter gut microbiota composition and promote the growth of beneficial bacteria, potentially through the synergistic actions of specific active components within the OMVs that regulate host immune systems and microbiota interactions. Transmission electron microscopy and negative staining confirmed the physical characteristics of Fp.OMVs. High-throughput sequencing analysis identified proteins, metabolites, and small RNAs in Fp.OMVs, including components known to regulate bacterial function. For example, indole, a microbial community signaling molecule, controls various aspects of bacterial physiology such as spore formation, plasmid stability, antibiotic resistance, and biofilm formation [42, 43]. These components may achieve antiviral effects by activating host immune cells,

(See figure on next page.)

Fig. 7 PC alleviates intestinal viral infection. **a** Analysis of PC content in the intestine of piglets. **b** Establishment of the PC function verification model; piglet small intestines were collected on day 5 post-infection for evaluation of intestinal damage. Groups included Abx + PC + PEDV ($n = 6$), Abx + PEDV ($n = 6$), and Control ($n = 6$). Comparative analysis of clinical indicators of survival (**c**), weight loss (**d**), and diarrhea (**g**) in each group of piglets. **e** Analysis of epithelial cell shedding based on pathological sections. **f** Scanning electron microscopy analysis of jejunal villi; images taken at 10×, 200×, and 500× magnifications. **h** Changes in the appearance of the intestines. **i** Comparison of histopathological changes (H&E staining); images taken at 20× and 100× magnifications. **j** Analysis of relative expression levels of PEDV in the intestines. **k** Characterization of viral content in intestinal epithelial cells using PEDV-N. **l** Immunofluorescence analysis of the intestines using PEDV-S; images taken at 100× magnification. Results are presented as means ± SD, with statistical significance determined by t tests for two groups and one-way ANOVA for three groups. *$P < 0.05$; **$P < 0.01$; ***$P < 0.001$. Panel **a** was created with BioRender.com

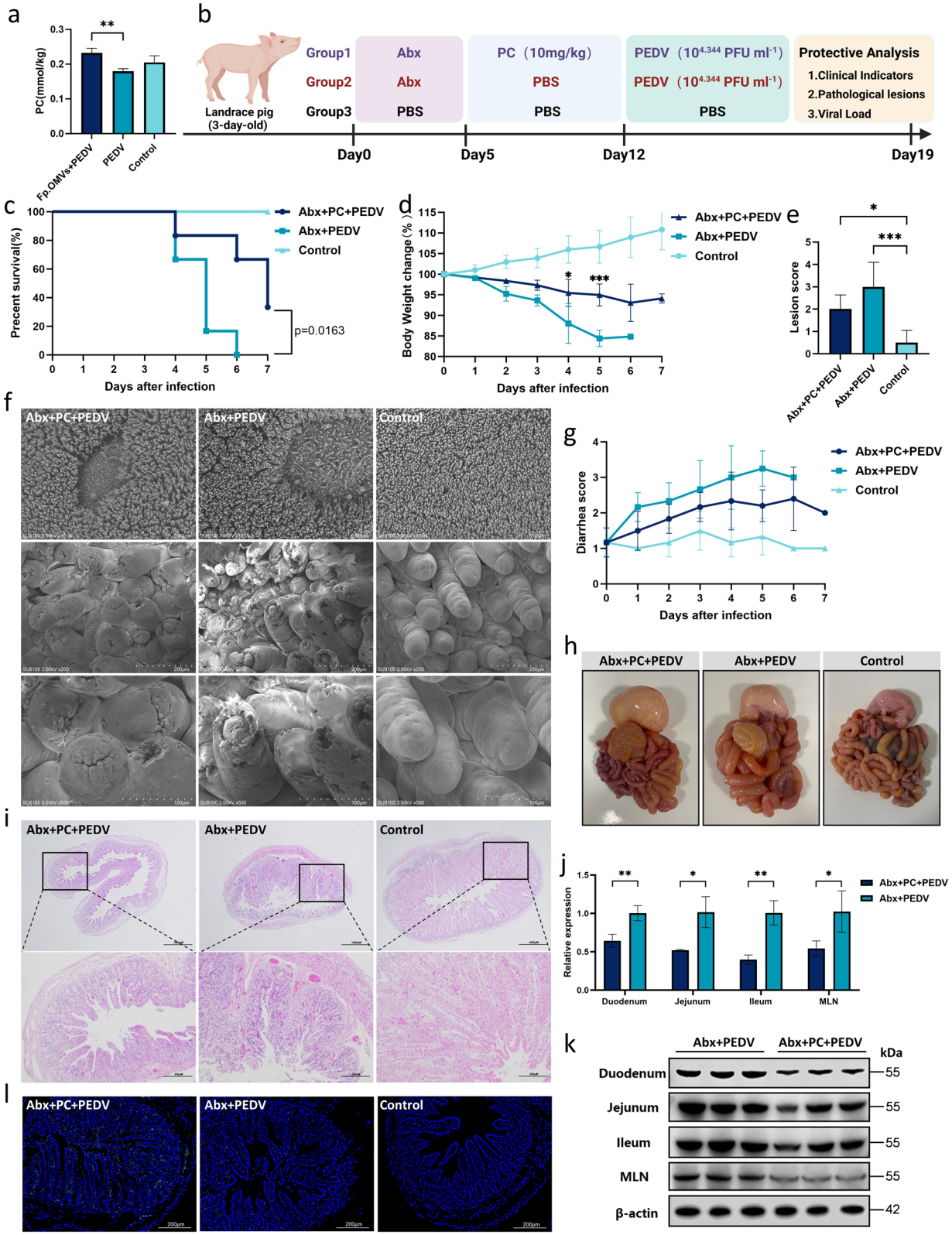

Fig. 7 (See legend on previous page.)

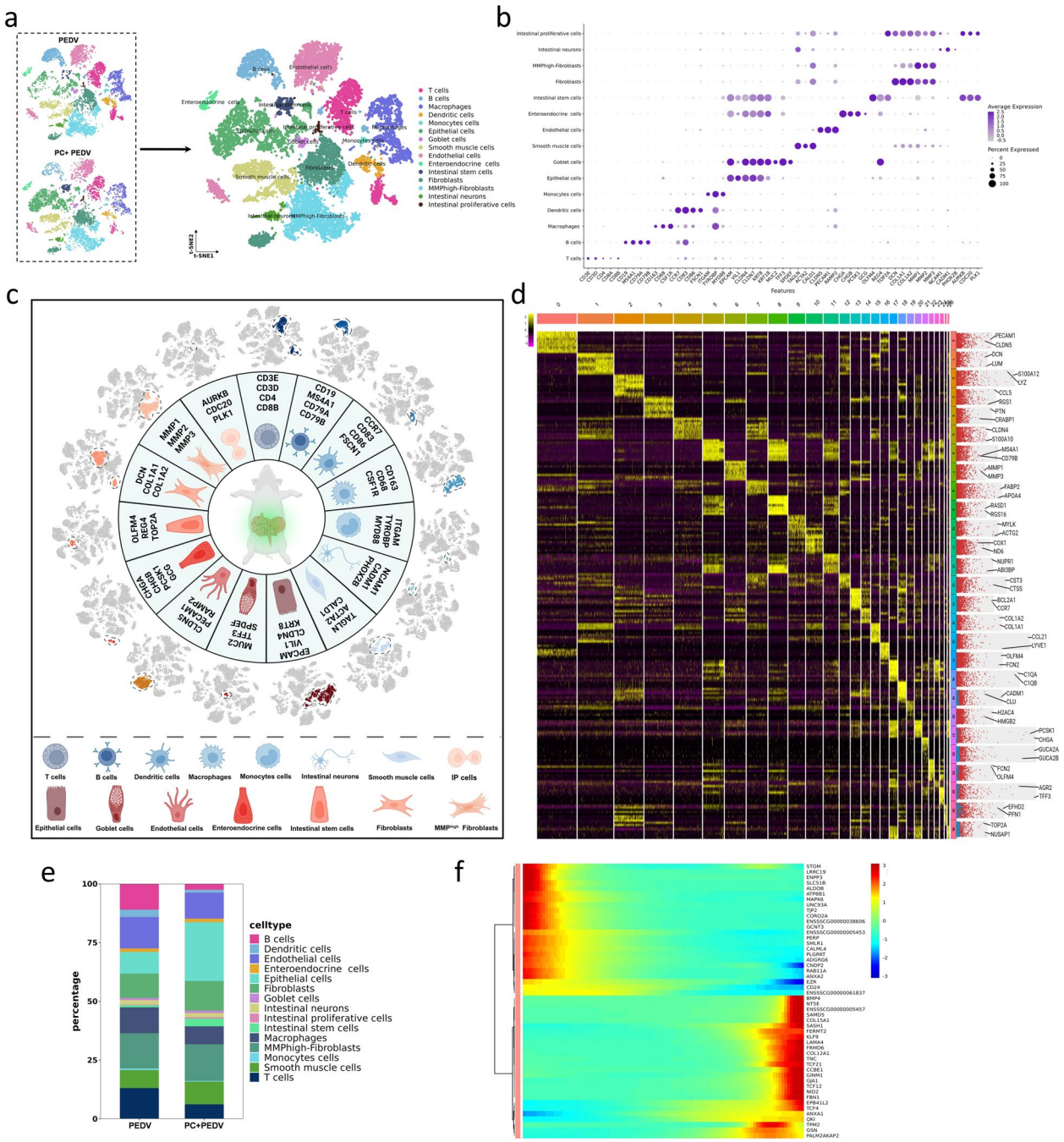

Fig. 8 PC regulates intestinal cell abundance and rescues a large number of epithelial cells during infection. **a** Single-cell sequencing analysis of intestinal cell distribution after PC treatment; dimensionality reduction analysis using the t-SNE algorithm. **b** Expression analysis of cell markers in different cell groups. **c** Integrated map of the location and markers of various cell types in piglets. **d** Volcano plot and heatmap analysis of marker genes in different cell groups, with $P \leq 0.01$ and gene expression fold change logFC ≥ 0.26. **e** Analysis of cell proportions in the PEDV and PC + PEDV groups. **f** Screening of highly expressed genes in early and late phases in intestinal cell groups. Panel **c** was created with BioRender.com

promoting the secretion of antiviral factors, or inhibiting key enzymes involved in viral replication.

We unexpectedly discovered that the antiviral function of Fp.OMVs relies on the presence of gut microbiota, which contrasts with previous studies where OMVs exerted direct regulatory effects [44–47]. The bacteria-OMVs-bacteria signaling pathway may be crucial in shaping the human microbiota's composition. The gut

microbiota, a complex ecosystem of trillions of microorganisms, is closely linked to the host's immune system, metabolic function, and overall health [48, 49]. Using an antibiotic-treated gut microbiota disruption model, we found that Fp.OMVs lost their function without a normal microbiota. The gut microbiota is essential for maintaining host health, and its integrity is vital for immune and metabolic functions [50]. Metagenomic analysis revealed that Fp.OMVs significantly altered the diversity and structure of the gut microbiota, particularly increasing the abundance of *Faecalibacterium prausnitzii*, *Prevotellamassilia timonensis*, and *Limosilactobacillus reuteri*. This highlights the importance of ecological balance in the microbiota for the antiviral function of Fp.OMVs. To further investigate this dependency, we cultured bacteria in vitro with varying concentrations of Fp.OMVs and observed significant growth promotion of *Faecalibacterium prausnitzii*, *Prevotellamassilia timonensis*, and *Limosilactobacillus reuteri*. Confocal microscopy with DIL labeling showed that Fp.OMVs can bind to these bacteria, suggesting direct intercellular interactions that affect bacterial growth and function. Flow cytometry further validated this, demonstrating that Fp.OMVs play a crucial regulatory role within bacterial communities. These findings provide important clues for future research in microbiota regulation.

Bacterial metabolism is crucial for growth and adaptation to various environmental conditions, such as different temperatures, pH levels, and oxygen concentrations. Bacterial metabolites are involved in mechanisms that combat infection and disease [38, 51]. Fp.OMVs significantly alter the metabolic profiles of gut and co-cultured bacteria, notably increasing levels of phosphatidylcholine (PC) metabolites, which are derived from synthesized and modified PC. PC is a typical eukaryotic membrane phospholipid found in only about 10% of all bacterial species, particularly those interacting with eukaryotes. There are two known pathways for PC biosynthesis in bacteria: the methylation pathway and the phosphatidylcholine synthase (Pcs) pathway [52]. Previous studies have shown that PC formation in bacteria is essential for symbiotic and pathogenic interactions. PC deficiency disrupts certain organisms' motility, bacterial growth, and stress responses [53, 54]. Our study discovered a new function of PC in improving clinical symptoms, reducing tissue damage, and lowering viral load during viral infections. Accumulation of PC on the mucosal surface is crucial for protecting colonic epithelial cells from pathogenic invasion [55]. Reduced PC in colonic mucus compromises the mucosal barrier, leading to attacks by commensal bacteria and inducing colitis. Clinical trials using PC as a novel therapeutic have shown promise in alleviating ulcerative colitis [56], suggesting its significant potential in treating gut diseases and viral infections.

Given PC's crucial role in the gut, analyzing how PC regulates gut cell function is essential. Although we previously explored cell distribution in a pig model [57], we defined gut cells more precisely and comprehensively by combining functional data from high-expression genes with human and mouse databases. Sequencing revealed that PC pretreatment significantly altered gut cell community distribution, notably increasing epithelial cell proportions. Epithelial cells are vital for gut barrier function and immune defense [58]. They also maintain host-microbe relationships and immune cell homeostasis in the gut [59]. Studies have shown that choline metabolites from PC synthesis and degradation regulate cell proliferation, growth, and programmed cell death [60], suggesting similar functions during viral infections. Subsequent functional pathway predictions for gut epithelial cells indicated that PC could inhibit necroptosis pathways. This finding was validated experimentally, showing that PC protects epithelial cells from virus-induced damage. Moreover, PC pretreatment significantly influenced interactions between gut cells. Cell signaling analysis revealed that PC regulates cell function and immune response through various receptor-ligand interactions, which might be a crucial pathway for PC in gut immune regulation.

In summary, Fp.OMVs act as communication vectors to regulate intestinal flora and metabolism, especially

(See figure on next page.)

Fig. 9 PC alleviates necroptosis caused by PEDV infection. **a** Statistical analysis of downregulated pathways in the cell growth and death (KEGG) category in intestinal epithelial cells after PC treatment. **b** Analysis of IPEC-J2 cell viability at varying PC concentrations (1, 5, 10, 20, 50, 100, 200, 500, 1000, 2000, 5000 μM). **c** Analysis of Vero cell viability at varying PC concentrations (1, 5, 10, 20, 50, 100, 200, 500, 1000, 2000, 5000 μM). **d** Flow cytometry analysis of the effect of different PC concentrations on IPEC-J2 and Vero cell death post-PEDV infection, with statistical analysis of differences in Q2 regions in IPEC-J2 (**e**) and Vero (**f**) cells, PC^{L},1 μM; PC^{M}, 5 μM; $PC.^{H}$, 10 μM. Flow cytometry detection of cell death in IPEC-J2 and Vero cells treated with PC alone or combined with inhibitors Nec-1 (20 μM) and GSK-872 (5 μM), with statistical analysis of differences in Q2 regions in IPEC-J2 (**h**) and Vero (**i**) cells. Expression analysis of RIPK1, p-RIPK1, RIPK3, p-RIPK3, MLKL, p-MLKL, and PEDV-N in IPEC-J2 (**j**) and Vero (**k**) cells pre-treated with various PC concentrations post-PEDV infection. Viability analysis of IPEC-J2 (**l**) and Vero (**m**) cells treated with PC (10 μM) alone or combined with inhibitors Nec-1 (20 μM) and GSK-872 (5 μM). Results are presented as means ± SD, with statistical significance calculated by one-way ANOVA for five groups. $^{*}P < 0.05$; $^{**}P < 0.01$; $^{***}P < 0.001$

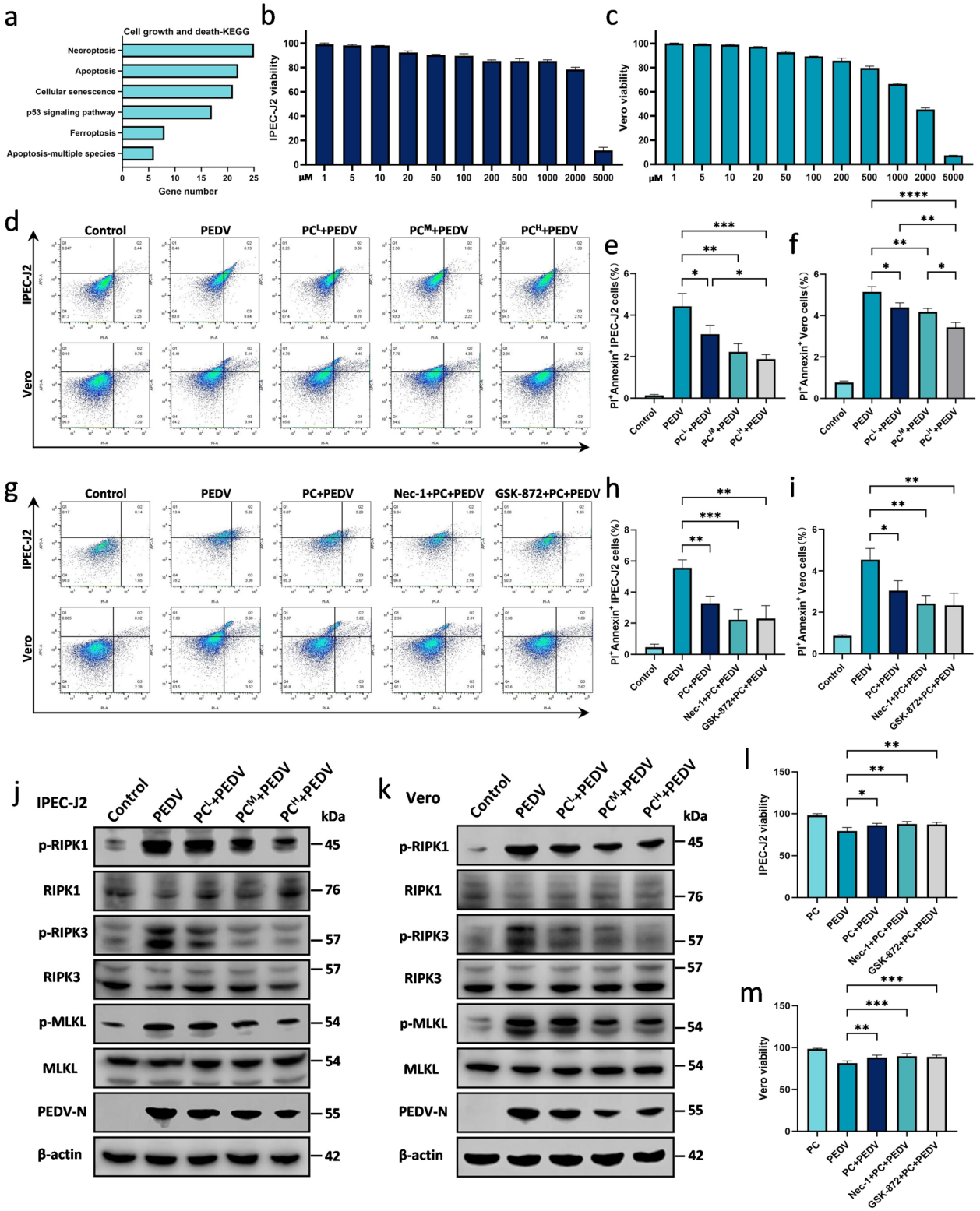

Fig. 9 (See legend on previous page.)

increasing PC metabolites, which significantly reduces pathological damage and viral load caused by PEDV infection. This discovery provides a theoretical basis for the development of PEDV prevention and treatment methods based on *F.prausnitzii*, and provides a new perspective on the relationship between intestinal flora and host health.

Supplementary Information

The online version contains supplementary material available at https://doi.org/10.1186/s40168-025-02078-x.

Supplementary Material 1.

Acknowledgements
We acknowledge the members of Jilin Provincial Engineering Research Center of Animal Probiotics, Jilin Provincial Key Laboratory of Animal Microecology and Healthy Breeding, Engineering Research Center of Microecological Vaccines (Drugs) for Major Animal Diseases, Ministry of Education, Jilin Agricultural University, Changchun, 130118, China. for their assistance with sampling and data analysis. We acknowledge Changchun Veterinary Research Institute, Chinese Academy of Agricultural Sciences, State Key Laboratory of Pathogen and Biosecurity, Key Laboratory of Jilin Province for Zoonosis Prevention and Control, Changchun, China, for their technical support for this study. We acknowledge Biorender (www.biorender.com) and Chiplot (www.chiplot.online) for providing the mapping platform.

Authors' contributions
C.F.W., W.T.Y., and G.L.Y. designed the experiments. J.H.X. wrote the paper. B.S.Z., and D.X.Z organized and typeset the images. T.M.N., C.W.S., and T.Y. helped with sample collection and data presentation. Y.J.W., S.H.F., M.H.L., and H.B.H. performed the majority of the experiments and analyzed the data. M.Y.B., Y.S., K.P.G., and J.J.Q. helped revise the manuscript. S.M.Z., J.Z.W., X.C., N.W., and Y.Z. supervised the study. Y.L.J., J.T.H., D.Z., and W.S.S. drafted the original paper. All authors read and approved the final manuscript.

Funding
This work was supported by the National Key R&D Program of China (2023YFD1800301, 2023YFD1800302), the National Natural Science Foundation of China (U21A20261, 32202819 and 32072888), the China Agriculture Research System of MOF and MARA (CARS-35), the Science and Technology Development Program of Jilin Province (YDZJ202301ZYTS326, YDZJ202102CXJD029, 20210202102NC, 20230202080NC, 20220202057NC, 20230101346JC and 20240601058RC).

Data availability
No datasets were generated or analysed during the current study.

Declarations

Ethics approval and consent to participate
The experimental procedures in this study were reviewed and authorized by the Animal Protection and Ethics Committee of Jilin Agricultural University (20240422001). The committee also monitored the adherence to established protocols throughout the process to ensure ethical compliance.

Consent for publication
Not applicable.

Competing interests
The authors declare no competing interests.

Author details
[1]College of Veterinary Medicine, Jilin Provincial Engineering Research Center of Animal Probiotics, Jilin Provincial Key Laboratory of Animal Microecology and Healthy Breeding, Engineering Research Center of Microecological Vaccines (Drugs) for Major Animal Diseases, Ministry of Education, Jilin Agricultural University, 2888 Xincheng Street, Changchun 130118, China.

Received: 28 October 2024 Accepted: 4 March 2025
Published online: 02 April 2025

References

1. Zhang H, Zou C, Peng O, Ashraf U, Xu Q, Gong L, et al. Global Dynamics of Porcine Enteric Coronavirus PEDV Epidemiology, Evolution, and Transmission. Mol Biol Evol. 2023;40(3):msad052. https://doi.org/10.1093/molbev/msad052.
2. Jung K, Saif LJ, Wang Q. Porcine epidemic diarrhea virus (PEDV): An update on etiology, transmission, pathogenesis, and prevention and control. Virus Res. 2020;286: 198045. https://doi.org/10.1016/j.virusres.2020.198045.
3. Machiels K, Joossens M, Sabino J, De Preter V, Arijs I, Eeckhaut V, et al. A decrease of the butyrate-producing species Roseburia hominis and Faecalibacterium prausnitzii defines dysbiosis in patients with ulcerative colitis. Gut. 2014;63(8):1275–83. https://doi.org/10.1136/gutjnl-2013-304833.
4. Schirmer M, Franzosa EA, Lloyd-Price J, McIver LJ, Schwager R, Poon TW, et al. Dynamics of metatranscription in the inflammatory bowel disease gut microbiome. Nat Microbiol. 2018;3(3):337–46. https://doi.org/10.1038/s41564-017-0089-z.
5. Sokol H, Pigneur B, Watterlot L, Lakhdari O, Bermúdez-Humarán LG, Gratadoux JJ, et al. Faecalibacterium prausnitzii is an anti-inflammatory commensal bacterium identified by gut microbiota analysis of Crohn disease patients. Proc Natl Acad Sci U S A. 2008;105(43):16731–6. https://doi.org/10.1073/pnas.0804812105.
6. Li HB, Xu ML, Xu XD, Tang YY, Jiang HL, Li L, et al. Faecalibacterium prausnitzii Attenuates CKD via Butyrate-Renal GPR43 Axis. Circ Res. 2022;131(9):e120–34. https://doi.org/10.1161/circresaha.122.320184.
7. Suskun C, Kilic O, Yilmaz Ciftdogan D, Guven S, Karbuz A, Ozkaya Parlakay A, et al. Intestinal microbiota composition of children with infection with severe acute respiratory syndrome coronavirus 2 (SARS-CoV-2) and multisystem inflammatory syndrome (MIS-C). Eur J Pediatr. 2022;181(8):3175–91. https://doi.org/10.1007/s00431-022-04494-9.
8. Gu S, Chen Y, Wu Z, Chen Y, Gao H, Lv L, et al. Alterations of the Gut Microbiota in Patients With Coronavirus Disease 2019 or H1N1 Influenza. Clin Infect Dis. 2020;71(10):2669–78. https://doi.org/10.1093/cid/ciaa709.
9. Al Khatib HA, Mathew S, Smatti MK, Eltai NO, Pathan SA, Al Thani AA, et al. Profiling of Intestinal Microbiota in Patients Infected with Respiratory Influenza A and B Viruses. Pathogens. 2021;10(6):761. https://doi.org/10.3390/pathogens10060761.
10. Wang K, Zhang Z, Mo ZS, Yang XH, Lin BL, Peng L, et al. Gut microbiota as prognosis markers for patients with HBV-related acute-on-chronic liver failure. Gut Microbes. 2021;13(1):1–15. https://doi.org/10.1080/19490976.2021.1921925.
11. Patin NV, Peña-Gonzalez A, Hatt JK, Moe C, Kirby A, Konstantinidis KT. The Role of the Gut Microbiome in Resisting Norovirus Infection as Revealed by a Human Challenge Study. mBio. 2020;11(6):e02634-20–20. https://doi.org/10.1128/mBio.02634-20.
12. Mutlu EA, Keshavarzian A, Losurdo J, Swanson G, Siewe B, Forsyth C, et al. A compositional look at the human gastrointestinal microbiome and immune activation parameters in HIV infected subjects. PLoS Pathog. 2014;10(2): e1003829. https://doi.org/10.1371/journal.ppat.1003829.
13. Nowak P, Troseid M, Avershina E, Barqasho B, Neogi U, Holm K, et al. Gut microbiota diversity predicts immune status in HIV-1 infection. AIDS. 2015;29(18):2409–18. https://doi.org/10.1097/qad.0000000000000869.
14. Spacova I, De Boeck I, Bron PA, Delputte P, Lebeer S. Topical Microbial Therapeutics against Respiratory Viral Infections. Trends Mol Med. 2021;27(6):538–53. https://doi.org/10.1016/j.molmed.2021.03.009.
15. Brown L, Wolf JM, Prados-Rosales R, Casadevall A. Through the wall: extracellular vesicles in Gram-positive bacteria, mycobacteria and fungi. Nat Rev Microbiol. 2015;13(10):620–30. https://doi.org/10.1038/nrmicro3480.
16. Chmiela M, Walczak N, Rudnicka K. Helicobacter pylori outer membrane vesicles involvement in the infection development and Helicobacter pylori-related diseases. J Biomed Sci. 2018;25(1):78. https://doi.org/10.1186/s12929-018-0480-y.

17. Kapteijn R, Shitut S, Aschmann D, Zhang L, de Beer M, Daviran D, et al. Endocytosis-like DNA uptake by cell wall-deficient bacteria. Nat Commun. 2022;13(1):5524. https://doi.org/10.1038/s41467-022-33054-w.
18. Dell'Annunziata F, Folliero V, Giugliano R, De Filippis A, Santarcangelo C, Izzo V, et al. Gene Transfer Potential of Outer Membrane Vesicles of Gram-Negative Bacteria. Int J Mol Sci. 2021;22(11):5985. https://doi.org/10.3390/ijms22115985.
19. Dell'Annunziata F, Dell'Aversana C, Doti N, Donadio G, Dal Piaz F, Izzo V, et al. Outer Membrane Vesicles Derived from Klebsiella pneumoniae Are a Driving Force for Horizontal Gene Transfer. Int J Mol Sci. 2021;22(16):8732. https://doi.org/10.3390/ijms22168732.
20. Chen Y, Ou Z, Pang M, Tao Z, Zheng X, Huang Z, et al. Extracellular vesicles derived from Akkermansia muciniphila promote placentation and mitigate preeclampsia in a mouse model. J Extracell Vesicles. 2023;12(5): e12328. https://doi.org/10.1002/jev2.12328.
21. Tao S, Fan J, Li J, Wu Z, Yao Y, Wang Z, et al. Extracellular vesicles derived from Lactobacillus johnsonii promote gut barrier homeostasis by enhancing M2 macrophage polarization. J Adv Res. 2024. https://doi.org/10.1016/j.jare.2024.03.011.
22. Kim W, Lee EJ, Bae IH, Myoung K, Kim ST, Park PJ, et al. Lactobacillus plantarum-derived extracellular vesicles induce anti-inflammatory M2 macrophage polarization in vitro. J Extracell Vesicles. 2020;9(1):1793514. https://doi.org/10.1080/20013078.2020.1793514.
23. de Vos WM, Tilg H, Van Hul M, Cani PD. Gut microbiome and health: mechanistic insights. Gut. 2022;71(5):1020–32. https://doi.org/10.1136/gutjnl-2021-326789.
24. Yang W, Yu T, Huang X, Bilotta AJ, Xu L, Lu Y, et al. Intestinal microbiota-derived short-chain fatty acids regulation of immune cell IL-22 production and gut immunity. Nat Commun. 2020;11(1):4457. https://doi.org/10.1038/s41467-020-18262-6.
25. Sun M, Wu W, Chen L, Yang W, Huang X, Ma C, et al. Microbiota-derived short-chain fatty acids promote Th1 cell IL-10 production to maintain intestinal homeostasis. Nat Commun. 2018;9(1):3555. https://doi.org/10.1038/s41467-018-05901-2.
26. Long SL, Gahan CGM, Joyce SA. Interactions between gut bacteria and bile in health and disease. Mol Aspects Med. 2017;56:54–65. https://doi.org/10.1016/j.mam.2017.06.002.
27. Sun J, Zhang Y, Kong Y, Ye T, Yu Q, Kumaran Satyanarayanan S, et al. Microbiota-derived metabolite Indoles induced aryl hydrocarbon receptor activation and inhibited neuroinflammation in APP/PS1 mice. Brain Behav Immun. 2022;106:76–88. https://doi.org/10.1016/j.bbi.2022.08.003.
28. Nishiyama-Naruke A, Curi R. Phosphatidylcholine participates in the interaction between macrophages and lymphocytes. Am J Physiol Cell Physiol. 2000;278(3):C554–60. https://doi.org/10.1152/ajpcell.2000.278.3.C554.
29. Xing JH, Niu TM, Zou BS, Yang GL, Shi CW, Yan QS, et al. Gut microbiota-derived LCA mediates the protective effect of PEDV infection in piglets. Microbiome. 2024;12(1):20. https://doi.org/10.1186/s40168-023-01734-4.
30. da Silva Barreira D, Lapaquette P, Novion Ducassou J, Couté Y, Guzzo J, Rieu A. Spontaneous Prophage Induction Contributes to the Production of Membrane Vesicles by the Gram-Positive Bacterium Lacticaseibacillus casei BL23. mBio. 2022;13(5):e0237522. https://doi.org/10.1128/mbio.02375-22.
31. Bae M, Cassilly CD, Liu X, Park SM, Tusi BK, Chen X, et al. Akkermansia muciniphila phospholipid induces homeostatic immune responses. Nature. 2022;608(7921):168–73. https://doi.org/10.1038/s41586-022-04985-7.
32. Wang L, Tang L, Feng Y, Zhao S, Han M, Zhang C, et al. A purified membrane protein from Akkermansia muciniphila or the pasteurised bacterium blunts colitis associated tumourigenesis by modulation of CD8(+) T cells in mice. Gut. 2020;69(11):1988–97. https://doi.org/10.1136/gutjnl-2019-320105.
33. Li J, Feng S, Wang Z, He J, Zhang Z, Zou H, et al. Limosilactobacillus mucosae-derived extracellular vesicles modulates macrophage phenotype and orchestrates gut homeostasis in a diarrheal piglet model. NPJ Biofilms Microbiomes. 2023;9(1):33. https://doi.org/10.1038/s41522-023-00403-6.
34. Díaz-Garrido N, Badia J, Baldomà L. Microbiota-derived extracellular vesicles in interkingdom communication in the gut. J Extracell Vesicles. 2021;10(13): e12161. https://doi.org/10.1002/jev2.12161.
35. Ñahui Palomino RA, Vanpouille C, Costantini PE, Margolis L. Microbiota-host communications: Bacterial extracellular vesicles as a common language. PLoS Pathog. 2021;17(5): e1009508. https://doi.org/10.1371/journal.ppat.1009508.
36. Wang G, Huang S, Wang Y, Cai S, Yu H, Liu H, et al. Bridging intestinal immunity and gut microbiota by metabolites. Cell Mol Life Sci. 2019;76(20):3917–37. https://doi.org/10.1007/s00018-019-03190-6.
37. Sencio V, Barthelemy A, Tavares LP, Machado MG, Soulard D, Cuinat C, et al. Gut Dysbiosis during Influenza Contributes to Pulmonary Pneumococcal Superinfection through Altered Short-Chain Fatty Acid Production. Cell Rep. 2020;30(9):2934-47.e6. https://doi.org/10.1016/j.celrep.2020.02.013.
38. Antunes KH, Fachi JL, de Paula R, da Silva EF, Pral LP, Dos Santos A, et al. Microbiota-derived acetate protects against respiratory syncytial virus infection through a GPR43-type 1 interferon response. Nat Commun. 2019;10(1):3273. https://doi.org/10.1038/s41467-019-11152-6.
39. Lamers MM, Beumer J, van der Vaart J, Knoops K, Puschhof J, Breugem TI, et al. SARS-CoV-2 productively infects human gut enterocytes. Science. 2020;369(6499):50–4. https://doi.org/10.1126/science.abc1669.
40. Lunney JK, Van Goor A, Walker KE, Hailstock T, Franklin J, Dai C. Importance of the pig as a human biomedical model. Sci Transl Med. 2021;13(621):eabd5758. https://doi.org/10.1126/scitranslmed.abd5758.
41. Prather RS, Lorson M, Ross JW, Whyte JJ, Walters E. Genetically engineered pig models for human diseases. Annu Rev Anim Biosci. 2013;1:203–19. https://doi.org/10.1146/annurev-animal-031412-103715.
42. Lee JH, Lee J. Indole as an intercellular signal in microbial communities. FEMS Microbiol Rev. 2010;34(4):426–44. https://doi.org/10.1111/j.1574-6976.2009.00204.x.
43. Lee JH, Wood TK, Lee J. Roles of indole as an interspecies and interkingdom signaling molecule. Trends Microbiol. 2015;23(11):707–18. https://doi.org/10.1016/j.tim.2015.08.001.
44. Chelakkot C, Choi Y, Kim DK, Park HT, Ghim J, Kwon Y, et al. Akkermansia muciniphila-derived extracellular vesicles influence gut permeability through the regulation of tight junctions. Exp Mol Med. 2018;50(2): e450. https://doi.org/10.1038/emm.2017.282.
45. He B, Wang H, Liu G, Chen A, Calvo A, Cai Q, et al. Fungal small RNAs ride in extracellular vesicles to enter plant cells through clathrin-mediated endocytosis. Nat Commun. 2023;14(1):4383. https://doi.org/10.1038/s41467-023-40093-4.
46. Luo ZW, Xia K, Liu YW, Liu JH, Rao SS, Hu XK, et al. Extracellular Vesicles from Akkermansia muciniphila Elicit Antitumor Immunity Against Prostate Cancer via Modulation of CD8(+) T Cells and Macrophages. Int J Nanomedicine. 2021;16:2949–63. https://doi.org/10.2147/ijn.S304515.
47. Wang S, He B, Wu H, Cai Q, Ramírez-Sánchez O, Abreu-Goodger C, et al. Plant mRNAs move into a fungal pathogen via extracellular vesicles to reduce infection. Cell Host Microbe. 2024;32(1):93-105.e6. https://doi.org/10.1016/j.chom.2023.11.020.
48. Shi N, Li N, Duan X, Niu H. Interaction between the gut microbiome and mucosal immune system. Mil Med Res. 2017;4:14. https://doi.org/10.1186/s40779-017-0122-9.
49. Brown EM, Clardy J, Xavier RJ. Gut microbiome lipid metabolism and its impact on host physiology. Cell Host Microbe. 2023;31(2):173–86. https://doi.org/10.1016/j.chom.2023.01.009.
50. Heintz-Buschart A, Wilmes P. Human Gut Microbiome: Function Matters. Trends Microbiol. 2018;26(7):563–74. https://doi.org/10.1016/j.tim.2017.11.002.
51. Wypych TP, Pattaroni C, Perdijk O, Yap C, Trompette A, Anderson D, et al. Microbial metabolism of L-tyrosine protects against allergic airway inflammation. Nat Immunol. 2021;22(3):279–86. https://doi.org/10.1038/s41590-020-00856-3.
52. Aktas M, Wessel M, Hacker S, Klüsener S, Gleichenhagen J, Narberhaus F. Phosphatidylcholine biosynthesis and its significance in bacteria interacting with eukaryotic cells. Eur J Cell Biol. 2010;89(12):888–94. https://doi.org/10.1016/j.ejcb.2010.06.013.
53. Conover GM, Martinez-Morales F, Heidtman MI, Luo ZQ, Tang M, Chen C, et al. Phosphatidylcholine synthesis is required for optimal function of Legionella pneumophila virulence determinants. Cell Microbiol. 2008;10(2):514–28. https://doi.org/10.1111/j.1462-5822.2007.01066.x.
54. Sohlenkamp C, López-Lara IM, Geiger O. Biosynthesis of phosphatidylcholine in bacteria. Prog Lipid Res. 2003;42(2):115–62. https://doi.org/10.1016/s0163-7827(02)00050-4.

55. Amadei F, Fröhlich B, Stremmel W, Tanaka M. Nonclassical Interactions of Phosphatidylcholine with Mucin Protect Intestinal Surfaces: A Microinterferometry Study. Langmuir. 2018;34(46):14046–57. https://doi.org/10.1021/acs.langmuir.8b03035.
56. Stremmel W, Hanemann A, Braun A, Stoffels S, Karner M, Fazeli S, et al. Delayed release phosphatidylcholine as new therapeutic drug for ulcerative colitis–a review of three clinical trials. Expert Opin Investig Drugs. 2010;19(12):1623–30. https://doi.org/10.1517/13543784.2010.535514.
57. Fan B, Zhou J, Zhao Y, Zhu X, Zhu M, Peng Q, et al. Identification of Cell Types and Transcriptome Landscapes of Porcine Epidemic Diarrhea Virus-Infected Porcine Small Intestine Using Single-Cell RNA Sequencing. J Immunol. 2023;210(3):271–82. https://doi.org/10.4049/jimmunol.2101216.
58. Okumura R, Takeda K. Roles of intestinal epithelial cells in the maintenance of gut homeostasis. Exp Mol Med. 2017;49(5): e338. https://doi.org/10.1038/emm.2017.20.
59. Peterson LW, Artis D. Intestinal epithelial cells: regulators of barrier function and immune homeostasis. Nat Rev Immunol. 2014;14(3):141–53. https://doi.org/10.1038/nri3608.
60. Ridgway ND. The role of phosphatidylcholine and choline metabolites to cell proliferation and survival. Crit Rev Biochem Mol Biol. 2013;48(1):20–38. https://doi.org/10.3109/10409238.2012.735643.

Publisher's Note